

Spectral Methods Applied to Axisymmetric

Thin Film Flows

MSc Research Dissertation

Naeemah Modhien

0213550K

Supervisor: Professor E. Momoniat

Centre for Differential Equations, Continuum Mechanics and Applications

Department of Computational and Applied Mathematics

University of the Witwatersrand

May 8, 2009

I declare that this dissertation is my own unaided work except where references have been made. It is being submitted for the degree of Masters of Science at the University of the Witwatersrand, Johannesburg. It has not been submitted before for any degree or examination at any other university.

Naeemah Modhien

Acknowledgements

I would like to thank my mentor, teacher and supervisor, Professor E. Momiati, for his understanding, support, compassion, time, help, patience, guidance and valuable criticism. I would also like to thank Professor Mason for his time, notes and advice.

The financial assistance of the National Research Foundation (NRF) towards this research is hereby acknowledged. Opinions expressed and conclusions arrived at, are those of the author and are not necessarily to be attributed to the NRF.

Dedication

I dedicate this Msc Dissertation to my parents and loving husband and daughter.

CONTENTS

1. <i>Introduction</i>	12
2. <i>Derivation of the model</i>	14
3. <i>Numerical Techniques</i>	21
3.1 Pseudospectral Methods	21
3.1.1 Hermite Pseudospectral Methods	23
3.1.2 Sinc Pseudospectral Methods	24
3.2 Finite Differences	25
3.3 MATLAB's built-in function	27
4. <i>Single slot injection/suction for gravity driven spreading</i>	28
5. <i>Single slot injection/suction with the effects of both gravity and rotation</i>	36
6. <i>Single slot suction with the effect of rotation only</i>	45
7. <i>Conclusion</i>	57

LIST OF FIGURES

2.1	<i>Co-ordinate System</i>	15
3.1	Schematic for <i>the method of lines</i>	22
4.1	<i>Top view of the substrate</i>	29
4.2	<i>Plot of v_n for different values of A and $L = 0.4$ where $r_0 = 0.5$</i>	30
4.3	<i>Plot of the numerical solution of (4.4) at $r_0 = 0.5$ and $L = 0.25$ for varying magnitudes of injection where $A = 0$, $A = 0.5$ and $A = 1$</i>	31
4.4	<i>Plot of the numerical solution of (4.4) at $r_0 = 0.5$ and $L = 0.25$ for varying magnitudes of suction where $A = 0$, $A = -0.5$ and $A = -1$</i>	32
4.5	<i>Plot of the numerical solution of (4.4) at $r_0 = 0.5$ for varying magnitudes of injection where $A = 0$, $A = 0.5$ and $A = 1$. The width of the slot is changed to $L = 0.5$</i>	33
4.6	<i>Plot of the numerical solution of (4.1) at $r_0 = 0.5$ for varying magnitudes of suction where $A = 0$, $A = -0.5$ and $A = -1$. The width of the slot is changed to $L = 0.5$</i>	34

-
- 5.1 *Plot of the numerical solution of (5.2) for $v_n = 0$ and the magnitude of rotation is varied where $\lambda = 0$, $\lambda = 0.5$ and $\lambda = 1$. 37*
- 5.2 *Plot of the numerical solution of (5.2) where $r_0 = 0.5$, $L = 0.25$, $A = 0.5$. The magnitude of the rotation is varied where $\lambda = 0$, $\lambda = 0.5$ and $\lambda = 1$ 38*
- 5.3 *Plot of the numerical solution of (5.2) where $r_0 = 0.5$, $L = 0.25$, $A = 1$. The magnitude of the rotation is varied where $\lambda = 0$, $\lambda = 0.5$ and $\lambda = 1$ 39*
- 5.4 *Plot of the numerical solution of (5.2) where $r_0 = 0.5$, $L = 0.25$, $A = -0.5$. The magnitude of the rotation is varied where $\lambda = 0$, $\lambda = 0.5$ and $\lambda = 1$ 40*
- 5.5 *Plot of the numerical solution of (5.2) where $r_0 = 0.5$, $L = 0.25$, $A = -1$. The magnitude of the rotation is varied where $\lambda = 0$, $\lambda = 0.5$ and $\lambda = 1$ 41*
- 5.6 *Plot of the numerical solution of (5.2) where $r_0 = 0.5$, $A = 1$ and varying magnitudes of rotation. The width of the slot is changed to $L = 0.5$ 42*
- 5.7 *Plot of the numerical solution of (5.2) where $r_0 = 0.5$, $A = -0.5$ and varying magnitudes of rotation. The width of the slot is changed to $L = 0.5$ 43*
- 6.1 *Plot of the numerical solution of (6.1) for $v_n = 0$ and the magnitude of rotation is varied where $\lambda = 0.1$, $\lambda = 0.5$ and $\lambda = 1$ 46*

6.2	<i>Plot of the numerical solution of (6.1) where $r_0 = 0.5$, $L = 0.25$, $A = -0.5$ and $A = -1$. The magnitude of the rotation is varied where $\lambda = 0.1$, $\lambda = 0.5$ and $\lambda = 1$.</i>	47
6.3	<i>Plot of the numerical solution of (6.1) where $r_0 = 0.5$, $A = -0.5$ and $A = -1$ and varying magnitudes of rotation. The width of the slot is changed to $L = 0.5$.</i>	47
6.4	<i>Parametric solution for $t=0,1,2,3,4$ and projection of the char- acteristic curves on the $(r-t)$-plane for $v_n = 0$.</i>	49
6.5	<i>Parametric solution and characteristic projection for varying slot widths.</i>	50
6.5	<i>Parametric solution and characteristic projection for varying slot widths (cont).</i>	51
6.6	<i>Parametric solution and characteristic projection comparing slot magnitude $A = -0.4$ with $A = -0.2$ (— — —).</i>	52
6.7	<i>Parametric solution and characteristic projection comparing slot position.</i>	54
6.7	<i>Parametric solution and characteristic projection comparing slot positions (cont).</i>	55

LIST OF TABLES

1	Nomenclature	11
---	------------------------	----

ABSTRACT

We employ numerical techniques to investigate the influence of slot injection/suction on the thin film axisymmetric flow of a Newtonian fluid subject to centrifugal and Coriolis forces, gravity and rotation. Surface tension effects are neglected. We obtain a nonlinear diffusion equation when modeling the spreading of the free surface of a thin film under gravity with blowing or suction at the base. When we model the spreading of the free surface of a thin film under both gravity and rotation with blowing or suction we obtain a nonlinear second order partial differential equation. A first order quasi-linear partial differential equation is obtained when modeling the thickness of the thin film under the effects of rotation only with blowing or suction at the base. We compare and contrast spectral methods with MATLAB built-in functions as well as finite differences. We also examine the effect that the slot has on the wave breaking process.

Nomenclature

r	radial coordinate	z	azimuthal coordinate
θ	angular coordinate	H	characteristic film height
L_c	characteristic length	U	characteristic fluid velocity
Re	Reynolds number	ν	kinematic viscosity
B	Bond number	Fr	Froude number, $U/(gH)^{\frac{1}{2}}$
r_0	position of the leading edge of the slot	L	slot width
A	magnitude of slot injection/suction	t	time
v_n	injection/suction velocity normal to substrate	u	radial velocity of fluid
v	azimuthal velocity of fluid	p	pressure of the fluid
h	free surface of thin film	Ro	Rossby number, $U/(L_c\Omega)$
E	Ekman number, $E = (\nu/\Omega)^{\frac{1}{2}}$	δ	aspect ratio, $\delta = H/L_c$
Ω	angular velocity of disk	ρ	density of the fluid
g	acceleration due to gravity	λ	ratio of rotational speed and gravity

Chapter 1

INTRODUCTION

The free surface flow of a liquid film on a rotating disk is an interesting fluid mechanics problem. It plays an important role in many technological processes, the most obvious being related to coating applications. Spin coating has been widely used in the manufacture of integrated circuits, optical mirrors, color television screens and magnetic disks for data storage [1, 15]. Spin coating is a process in which a liquid is initially applied to a disk as a thick layer and then thinned by spinning the disk quickly [1, 6].

There have been a number of investigations in rotating thin film flows where numerous forces such as friction applied by the disk, centrifugal and Coriolis forces as a result of rotation, inertia and shear stress due to air/vapour act on the system (Acrivos *et al.*⁷, Meyerhofer⁴, Sukanek⁵, Hwang and Ma³).

In this dissertation we employ numerical techniques to investigate the influence of slot injection/suction on the thin film axisymmetric flow of a Newtonian fluid subject to centrifugal and Coriolis forces, gravity and rotation. Surface tension effects are neglected. We obtain a nonlinear diffusion equation when modeling the spreading of the free surface of a thin film under gravity with blowing or suction at the base. When we model the spreading of the free surface of a thin film under both gravity and rotation with blowing or suction we obtain a nonlinear second order partial differential equation. A first order quasi-linear partial differential

equation is obtained when modeling the thickness of the thin film under the effects of rotation only with blowing or suction at the base.

Uniform slot injection/suction has some important industrial applications in inkjet printing and the spreading of fluids on textiles and in the investigation of the runoff of rainwater over soils [27, 28]. Slot injection/suction has also been used to make the flow around an obstacle become stable [12].

In chapter 2, we derive the governing equations for thin film flow on a rotating substrate with suction/blowing at the base.

In chapter 3, we discuss the numerical techniques that will be used to solve our equations.

In chapter 4, we consider numerical solutions of the nonlinear diffusion equation governing the evolution of the free surface profile under gravity only.

In chapter 5, we consider numerical solutions of the nonlinear second order partial differential equation governing the evolution of the free surface profile under both gravity and rotation.

In chapter 6, we consider numerical solutions of the quasi-linear partial differential equation governing the evolution of the free surface profile under rotation only.

Concluding remarks are made in chapter 7.

Chapter 2

DERIVATION OF THE MODEL

In this chapter we derive the partial differential equation modeling the influence of slot injection/suction on the thin film axisymmetric flow of a Newtonian fluid subject to centrifugal and Coriolis forces, gravity and rotation. Surface tension effects are neglected.

To derive the governing equation for thin film flow on a rotating substrate with suction/blowing at the base, the standard lubrication Reynolds number approximate to the Navier-Stokes equation must be used to provide a single equation for the height $h(r, t)$ [15]. We use cylindrical polar co-ordinates (r, θ, z) , where r measures the radial distance from the center of the disk, θ is the angle from some fixed radial line in the disk and z measures the distance vertically upward from the solid surface of the disk [6, 15]. The physical set-up and co-ordinate system for the model are shown in Figure 2.1.

Forces acting on the thin liquid film are gravity, viscous resistance, centrifugal and Coriolis forces. We make the following assumptions to derive our model [15]:

- The disk is smooth and rotates about a vertical axis with constant angular velocity Ω ,
- The disk has an infinite radius so that edge effects are confined to a small region of the total film area and can therefore be neglected,
- The thin film is axisymmetric about the axis of rotation, this implies that

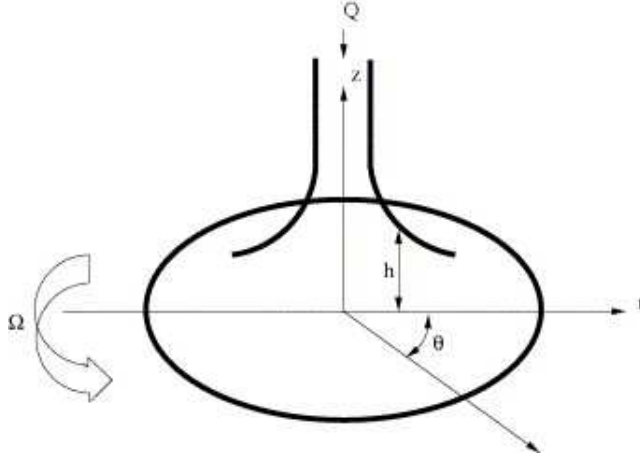


Fig. 2.1: Co-ordinate System

all quantities are independent of θ and that $\frac{\partial}{\partial \theta}(\bullet) = 0$,

- The fluid is incompressible, Newtonian and solvent free,
- In lubrication theory the aspect ratio of the flow, $\delta = H/L_c$ is small, so that $\delta^2, \delta^2 Re \ll 1$ and $Re = UL/\nu$ is the Reynolds number and ν is the kinematic viscosity. This means that derivatives in the direction perpendicular to the flow dominate and that the inertia terms may be neglected,
- There is no slip between the solid and the fluid,
- The shear stress at the free surface of the fluid caused by the airflow [14] and the evaporation at the liquid-gas interface [6] are negligible.

As given in Myers [15], the radial, r , azimuthal, θ , and z -components of the Navier-stokes equation in non-dimensional form for an axisymmetric thin film are:

$$\delta^2 Re \frac{du}{dt} = -\frac{PH^2}{\mu UL} \frac{\partial p}{\partial r} + \frac{\partial^2 u}{\partial z^2} + \frac{\rho \Omega^2 LH^2}{\mu U} r + \frac{2\rho \Omega V H^2}{\mu U} v + O(\delta^2), \quad (2.1)$$

$$\delta^2 Re \frac{dv}{dt} = \frac{\partial^2 v}{\partial z^2} - \frac{2\rho \Omega U H^2}{\mu V} u + O(\delta^2), \quad (2.2)$$

$$\delta^4 Re \frac{dw}{dt} = -\frac{PH^2}{\mu UL} \frac{\partial p}{\partial z} - \delta^3 \frac{\rho g L^2}{\mu U} + O(\delta^2). \quad (2.3)$$

Characteristic length scales for flow in the vertical and horizontal directions are the initial film thickness H and the disk radius L_c respectively and $\delta = H/L_c$. p is the fluid pressure and the corresponding scale $P = \mu UL_c/H^2$ agrees with the characteristic pressure used in thin film theory, w is the vertical velocity and the corresponding scales is W . The kinematic viscosity $\nu = \mu/\rho$ where ρ is the density. In the radial direction, the centrifugal force is the main driving force, the velocity scale is therefore $U = \Omega^2 L_c H^2/\nu$. In the azimuthal direction the driving force is the Coriolis force, so $V = 2\Omega U H^2/\nu$. The time scale is chosen as $\tau = L_c/U$ and the velocity-scale in the z-direction is $W = UH/L_c$ thus leaving the axisymmetric continuity equation unchanged

$$\frac{1}{r} \frac{\partial (ru)}{\partial r} + \frac{\partial w}{\partial z} = 0. \quad (2.4)$$

In dimensionless form the Navier-Stokes equations are

$$\left(\frac{H}{E}\right)^4 \frac{du}{dt} = -\frac{\partial p}{\partial r} + \frac{\partial^2 u}{\partial z^2} + r + 4\left(\frac{H}{E}\right)^4 v, \quad (2.5)$$

$$\left(\frac{H}{E}\right)^4 \frac{dv}{dt} = \frac{\partial^2 v}{\partial z^2} - u, \quad (2.6)$$

$$\delta^2 \left(\frac{H}{E}\right)^4 \frac{dw}{dt} = -\frac{\partial p}{\partial z} - B. \quad (2.7)$$

$B = gH/L_c^2\Omega^2$ is the Bond number and E is the thickness of the Ekman boundary layer in a rotating fluid, $E = \sqrt{\nu/\Omega}$. Diffusion increases the thickness of the Ekman boundary layer while rotation decreases the thickness. The ratio $(H/E)^4$ may be expressed in terms of the Reynolds number Re ,

$$\begin{aligned}
Re \left(\frac{H}{L_c} \right)^2 &= \frac{UL_c H^2}{\nu L_c^2} \\
&= \frac{\Omega^2 L_c H^2}{\nu} \frac{L_c H^2}{\nu L_c^2} \quad \left(\text{using } U = \frac{\Omega^2 L_c H^2}{\nu} \right) \\
&= \frac{\Omega^2}{\nu^2} H^4 \\
&= \left(\frac{H}{E} \right)^4 \quad \left(E = \left(\frac{\nu}{\Omega} \right)^{\frac{1}{2}} \right). \tag{2.8}
\end{aligned}$$

However in lubrication theory we require that $H/L_c \ll 1$, and $\delta^2 Re = Re(H/L_c)^2 = (H/E)^4 \ll 1$, thus resulting in the Coriolis force term in (2.5) to be neglected as it has the same order of magnitude as the inertia term.

Equations (2.5)-(2.7) are solved subject to the following boundary conditions:

At $z = 0$ we have the no slip boundary condition that the viscous fluid sticks to the disk,

$$u(r, 0, t) = v(r, 0, t) = 0. \tag{2.9}$$

A normal velocity, v_n , at the surface of the disk is induced by the injection/suction.

We thus have

$$w(r, 0, t) = v_n. \tag{2.10}$$

At the free surface of the fluid, $z = h(r, t)$, the kinematic condition holds which ensures that fluid particles on the free surface must remain on the free surface [24],

$$w(r, h, t) = \frac{\partial h}{\partial t} + u(r, h, t) \frac{\partial h}{\partial r}. \tag{2.11}$$

At the free surface $z = h(r, t)$, the fluid pressure equals the constant atmospheric pressure p_0 (surface tension is neglected),

$$p(r, h, t) = p_0. \tag{2.12}$$

On the free surface we neglect the effects of surface shear

$$\left. \frac{\partial u}{\partial z} \right|_{z=h(t,r)} = 0. \quad (2.13)$$

We use the continuity equation (2.4) to eliminate $w(r, h, t)$ from the kinematic condition (2.11). Integrate equation (2.4) with respect to z from $z = 0$ to $z = h(r, t)$,

$$\begin{aligned} \int_0^{h(r,t)} \frac{\partial w}{\partial z}(r, z, t) dz &= -\frac{1}{r} \int_0^{h(r,t)} \frac{\partial}{\partial r}(ru) dz, \\ w(r, h, t) - w(r, 0, t) &= -\frac{1}{r} \int_0^{h(r,t)} \frac{\partial}{\partial r}(ru) dz. \end{aligned} \quad (2.14)$$

But from boundary condition (2.10), we get $w(r, 0, t) = v_n$. Thus (2.14) becomes

$$w(r, h, t) = -\frac{1}{r} \int_0^{h(r,t)} \frac{\partial}{\partial r}(ru(r, z, t)) dz + v_n. \quad (2.15)$$

We have to differentiate under the integral sign. To do this we use the result [2]

$$\frac{d}{dx} \int_{\phi_1(x)}^{\phi_2(x)} f(x, y) dy = \int_{\phi_1(x)}^{\phi_2(x)} \frac{\partial}{\partial x} f(x, y) dy + f(x, \phi_2(x)) \phi_2'(x) - f(x, \phi_1(x)) \phi_1'(x)$$

Hence we obtain

$$\frac{\partial}{\partial r} \int_0^{h(r,t)} ru(r, z, t) dz = \int_0^{h(r,t)} \frac{\partial}{\partial r}(ru) dz + ru(r, h, t) \frac{\partial h}{\partial r}, \quad (2.16)$$

and therefore

$$\int_0^{h(r,t)} \frac{\partial}{\partial r}(ru) dz = \frac{\partial}{\partial r} \left(r \int_0^{h(r,t)} ru(r, z, t) dz \right) - ru(r, h, t) \frac{\partial h}{\partial r}. \quad (2.17)$$

Substitute (2.17) into (2.15) to obtain

$$w(r, h, t) = -\frac{1}{r} \frac{\partial}{\partial r} \left(r \int_0^{h(r,t)} ru(r, z, t) dz \right) + u(r, h, t) \frac{\partial h}{\partial r} + v_n. \quad (2.18)$$

We eliminate $w(r, h, t)$ from the kinematic condition (2.11) by substituting in the above expression to obtain

$$\frac{\partial h}{\partial t} + \frac{1}{r} \frac{\partial}{\partial r} \int_0^{h(t,r)} rv_r(r, z, t) dz = v_n. \quad (2.19)$$

Integrating (2.7) subject to (2.12) we obtain the leading order pressure for the fluid

$$p(r, h, t) = p_0 - B(z - h). \quad (2.20)$$

The expressions for the fluid velocities may be obtained by integrating (2.5) and (2.6) subject to the above boundary conditions

$$u(r, z, t) = \frac{1}{2} \left(\frac{\partial p}{\partial r} - r \right) (z^2 - 2hz), \quad (2.21)$$

$$v(r, z, t) = \frac{1}{24} \left(\frac{\partial p}{\partial r} - r \right) z (z^3 + 8h^3 - 4hz^2). \quad (2.22)$$

Finally by substituting u from (2.21) into (2.19), we obtain the expression

$$\frac{\partial h}{\partial t} = \frac{1}{3r} \frac{\partial}{\partial r} \left(Brh^3 \frac{\partial h}{\partial r} - r^2 h^3 \right) + v_n, \quad (2.23)$$

By dividing through by the Bond number B , we obtain the free surface equation which we will be considering in the course of this dissertation,

$$\frac{\partial h}{\partial t} = \frac{1}{3r} \frac{\partial}{\partial r} \left(rh^3 \frac{\partial h}{\partial r} - \lambda r^2 h^3 \right) + v_n, \quad (2.24)$$

where

$$\lambda = (Fr/Ro)^2, \quad (2.25)$$

is a ratio of the Froude and Rossby number, which measures the ratio of the rotational speed of the disk and gravitational acceleration.

By making appropriate approximations to equation (2.24) we are able to derive our equation for spreading under rotation with no gravity and spreading under gravity with no rotation. A difficulty that arises with this form of equation is whenever $h \rightarrow 0$, a nonintegrable singularity occurs [15, 16]. This usually occurs as a result of applying the no-slip boundary condition and occurs at the front

of the film droplet and they introduce the added complication of contact angles and moving contact lines [15, 16]. The interested reader is referred to [17–20] for literature on the moving contact line problem. Two of the simplest methods to deal with this is to use a Navier slip condition or one can allow a very thin film to precede the bulk of the fluid to surmount for the singularity which arises as a consequence of applying the no-slip boundary condition.

We consider the initial curve

$$h(r, 0) = \exp(-r^2). \quad (2.26)$$

We chose this initial profile so that we do not have to include numerical precursor film [14]. We solve the model equation (2.24) subject to the boundary conditions

$$\frac{\partial h(0, t)}{\partial r} = 0, \quad (a) \quad h(\infty, t) = 0 \quad (b). \quad (2.27)$$

The boundary condition (2.27a) is a result of the film being axisymmetric while the boundary condition (2.27b) fixes the height at the edge of the disk.

Chapter 3

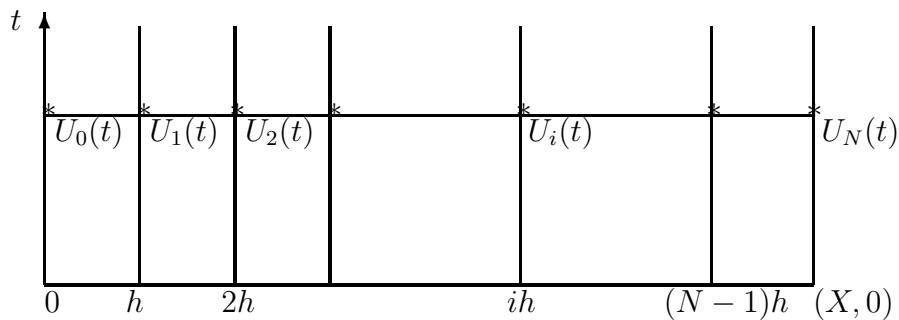
NUMERICAL TECHNIQUES

In this chapter we discuss a variety of numerical tools for solving the partial differential equation for the free surface profile. They include *the method of lines* coupled with pseudospectral methods (spectral collocation) and finite differences as well as built in **MATLAB** functions.

Our calculations are based on the notion of *the method of lines*. When a partial differential equation depends on both time and space and we only discretize the partial differential equation in terms of its space variable whether by a spectral method or any other method (finite differences), we obtain a system of ordinary differential equations in time. The idea of *the method of lines* is to integrate this coupled system of ordinary differential equations in the time variable by an integrator (Adams, Runge-Kutta, etc) [25]. By making use of *the method of lines*, the algebraic solutions obtained generates the solution from one time row to another in a step-by-step manner, see Figure 3.1.

3.1 Pseudospectral Methods

Spectral methods are known to be the best tool for achieving high accuracy for problems with smooth data and they use less computer memory as compared to finite difference or finite element methods [23, 25].

Fig. 3.1: Schematic for *the method of lines*.

Global spectral methods have been used in the application of climate modeling and weather forecasting while oceanography, image reconstruction and quantum chemistry are applications of multidomain spectral methods. Numerous references on the use of spectral methods in the modeling of turbulence can be found in Canuto et al. [22, 26].

Certain boundary conditions and irregular domains may cause difficulties or inefficiencies when using spectral methods [22, 23].

Spectral methods are global in that the function that we want to differentiate is approximated by a sum of very smooth basis functions

$$u(x) \approx \sum_{k=0}^N a_k \phi_k(x), \quad (3.1)$$

and in the case of a time-dependent problem, $u(x, t)$ is approximated by $v(x, t)$ and $a_k(t)$ [22]. We use a pseudospectral collocation method to determine the coefficients a_k . They are selected so that the boundary conditions are satisfied but the residual is zero at as many spatial points as possible.

Spectral collocation is based on interpolants of the form [22, 29]

$$f(x) \approx p_{N-1}(x) = \sum_{j=1}^N \frac{\alpha(x)}{\alpha x_j} \phi_j(x) f(x_j). \quad (3.2)$$

Here $\alpha(x)$ is a weight function, $x_j, j = 1, \dots, N$ is the set of distinct interpolation nodes and the interpolating functions ϕ_j satisfies $\phi_j(x_i) = \delta_{ji}$ (the Kronecker delta).

By differentiating (3.2) k times and evaluating the result at the nodes x_i , we obtain the collocation derivative operator:

$$f^k(x_i) \approx \sum_{j=1}^N \frac{d^k}{dx^k} \left[\frac{\alpha(x)}{\alpha(x_j)} \phi_j(x) \right]_{x=x_i} f(x_j), \quad i = 1, \dots, N. \quad (3.3)$$

An alternate representation of the derivative operator is as a differentiation matrix, D^k , as this is the form we will be using during our numerical computations

$$D_{i,j}^k = \frac{d^k}{dx^k} \left[\frac{\alpha(x)}{\alpha(x_j)} \phi_j(x) \right]_{x=x_i}. \quad (3.4)$$

3.1.1 Hermite Pseudospectral Methods

This pseudospectral method uses Hermite interpolation polynomials to approximate a function. It is used for problems posed on an infinite domain, i.e. $x \in (-\infty, \infty)$.

- The basis set of this method is defined by

$$\varphi_n(x) = e^{0.5x^2} H_n(x). \quad (3.5)$$

where the $H_n(x)$ is the Hermite polynomial of degree n and $e^{0.5x^2}$ is the weight function $\alpha(x)$.

- The Hermite polynomials $H_n(x)$ can be obtained through the three-term recurrence relation

$$H_0(x) = 1 \quad H_1(x) = 2x \quad H_{n+1}(x) = 2xH_n(x) - 2nH_{n-1}(x) \quad (3.6)$$

where $n = 1, 2, \dots$

- The derivative of $H_n(x)$ is simply $\frac{dH_n}{dx} = 2nH_{n-1}(x)$ for all n [22, 23].
- The interpolant is given as [29]

$$p_{N-1}(x) = \sum_{j=1}^N \frac{e^{-x^2/2}}{e^{-x_j^2/2}} \phi_j(x) f(x_j),$$

where

$$\phi_j(x) = \frac{H_N(x)}{H'_N(x_j)(x - x_j)}.$$

3.1.2 Sinc Pseudospectral Methods

The sinc pseudospectral method may be summarized as follows [29–31]:

- It is intended for solving problems on the real line $x \in (-\infty, \infty)$, however it may also be applied to the intervals $[0, \infty)$ and $[a, b]$.
- The space variable is discretized into equidistant points with spacing h , which are symmetric with respect to the origin

$$x_k = \left(k - \frac{N+1}{2}\right) h, \quad k = 1, \dots, N. \quad (3.7)$$

- The weight function is $\alpha(x) = 1$.
- By means of Sinc functions the dependent variable $u = u(x, t)$ is interpolated and approximated by the values $u_i(t) = u(t, x_i)$ as follows:

$$u(t, x) \cong u^N(t, x) = \sum_{j=1}^N S_j(x; h) u_j(t), \quad (3.8)$$

where $u_j(t) = u(t, x_j)$ and

$$S_j(x; h) = \frac{\sin((\pi/h)(x - jh))}{(\pi/h)(x - jh)}.$$

- We then use the interpolation defined above to approximate the partial derivatives of the variable u at the nodal points

$$\frac{\partial^r u}{\partial x^r}(t, x_i) \cong \sum_{j=1}^N \frac{d^r S_j}{dx^r}(x_i) u_j(t) = \sum_{j=1}^N a_{ji}^{(r)} u_j(t), \quad (3.9)$$

where $r=1, 2, \dots$

- All Sinc derivative matrices are constant along the diagonals (Toeplitz) and the first and second differentiation matrices are given as [29, 32]:

$$D^{(1)} = \frac{1}{h} \begin{bmatrix} 0 & 1 & -\frac{1}{2} & \dots & \frac{(-1)^N}{N-1} \\ -1 & 0 & 1 & & \\ \frac{1}{2} & -1 & 0 & & -\frac{1}{2} \\ & & & \ddots & 1 \\ \frac{(-1)^{N-1}}{N-1} & \dots & \frac{1}{2} & -1 & 0 \end{bmatrix} \quad (3.10)$$

$$D^{(2)} = \frac{1}{h^2} \begin{bmatrix} \frac{-\pi^2}{3} & 2 & -\frac{1}{2} & \dots & \frac{2(-1)^N}{(N-1)^2} \\ 2 & \frac{-\pi^2}{3} & 2 & & \\ -\frac{1}{2} & 2 & \frac{-\pi^2}{3} & & -\frac{1}{2} \\ & & & \ddots & 2 \\ \frac{2(-1)^N}{(N-1)^2} & \dots & -\frac{1}{2} & 2 & \frac{-\pi^2}{3} \end{bmatrix} \quad (3.11)$$

Since our problem is posed on a semi infinite domain, it is better to use Hermite and Sinc basis sets as opposed to Chebyshev and Fourier polynomials as they are associated with problems posed on a finite interval. A Chebyshev series is just a Fourier cosine expansion with a change of variable.

3.2 Finite Differences

We replace each derivative of the partial differential equation by a finite difference equation at the nodal points and obtain algebraic equations which we solve for the

unknowns [34]. Finite difference methods approximate derivatives of a function by local arguments, such as $du(x)/dx = [u(x+k) - u(x)]/k$, where k is a small grid spacing. We partition the interval $[a, b]$ into N equal parts of width k , $x_i = a + ik, i = 0, 1, \dots, N$ and $Nk = b$ and write down our equation at every mesh point. For the purposes of our computation the grid spacing will be chosen as $k = \frac{3}{N}$ where N is the number of subintervals that our spatial variable will be partitioned into. We will use central differences to approximate our first and second derivatives, i.e.

$$\begin{aligned}\frac{\partial h[r, t]}{\partial r} &= \frac{h[r+k, t] - h[r-k, t]}{2k}, \\ \frac{\partial^2 h[r, t]}{\partial r^2} &= \frac{h[r+k, t] - 2h[r, t] + h[r-k, t]}{k^2}.\end{aligned}\quad (3.12)$$

However since we are using *the method of lines*, we write $h(ik, t) = h_i(t)$ so that (3.12) becomes

$$\begin{aligned}\frac{dh_i(t)}{dr} &= \frac{h_{i+1}(t) - h_{i-1}(t)}{2k}, \\ \frac{d^2h_i(t)}{dr^2} &= \frac{h_{i+1}(t) - 2h_i(t) + h_{i-1}(t)}{k^2}.\end{aligned}\quad (3.13)$$

For stability criteria of finite difference methods for partial differential equations one may refer to Smith [34] and for stability criteria for pseudospectral methods one may refer to Fornberg [22] and Boyd [23]. The advantage of finite difference methods over pseudospectral methods is that they produce sparse matrix equations which use less computation time to be solved as opposed to the full matrices produced by the pseudospectral methods.

We notice that from the discretization and interpolation techniques described above we obtain a system of differential equations that are stiff, as the variables u_i are contained in each equation and so we make use of MATLAB's built-in function *ode15s* [21] to solve the system of ordinary differential equations.

3.3 MATLAB's built-in function

Since our partial differential equations obtained in chapter 2 consist of one space variable and time, we shall use MATLAB's partial differential solver **pdepe** to solve our system of equations. By using second order approximations to discretize the spatial variable [33], the **pdepe** solver converts the partial differential equations to ordinary differential equations and the time integration is done with *ode15s*.

The numerical techniques discussed above will be implemented under identical conditions so that comparisons of the different methods may be made and the final time, t_{final} , shall be chosen as 1. The package, a MATLAB Differentiation Matrix Suite [29] will be used to calculate the Sinc and Hermite differentiation matrices. The semi-infinite domain will also be approximated by the domain $r \in [0, r_{max}]$ where $h(r_{max}, t) \approx 0$. The boundary condition (2.27b) is replaced with

$$h(\infty, t) \approx h(r_{max}, 0) = e^{-r_{max}^2}. \quad (3.14)$$

The boundary condition (3.14) imposes a precursor film height [14] of $e^{-r_{max}^2}$ to avoid the singularity at $h = 0$. For all the plots, r_{max} is chosen as $r_{max} = 3$.

Chapter 4

SINGLE SLOT INJECTION/SUCTION FOR GRAVITY DRIVEN SPREADING

In this chapter we consider the effects of injection/suction on the free surface profile of the thin film when gravity alone is the driving force by employing the various numerical techniques discussed in chapter 3.

A nonlinear second-order partial differential equation models the spreading of the thin film when gravity alone is the driving force. This equation is obtained by letting $\lambda \rightarrow 0$ in (2.24)

$$\frac{\partial h}{\partial t} = \frac{1}{3r} \frac{\partial}{\partial r} \left(rh^3 \frac{\partial h}{\partial r} \right) + v_n. \quad (4.1)$$

There is a complication at $r = 0$. The term at $r = 0$ is indeterminate

$$\lim_{r \rightarrow 0} \frac{1}{r} \frac{\partial}{\partial r} = \frac{0}{0}. \quad (4.2)$$

If we apply L'Hopital's rule to the indeterminate form by differentiating the numerator and denominator with respect to r , we get

$$\lim_{r \rightarrow 0} \frac{1}{r} \frac{\partial}{\partial r} = \lim_{r \rightarrow 0} \frac{1}{1} \frac{\partial^2}{\partial r^2} = \frac{\partial^2}{\partial r^2}. \quad (4.3)$$

By using the approximation in (4.3), the equation at $r = 0$ can be replaced so that

the equation for the free surface profile is given as

$$\frac{\partial h}{\partial t} = \begin{cases} h^2 \left(\frac{\partial h}{\partial r} \right)^2 + \frac{2}{3} h^3 \frac{\partial^2 h}{\partial r^2} + v_n, & r = 0, \\ \frac{1}{3} \frac{h^3}{r} \frac{\partial h}{\partial r} - h^2 \left(\frac{\partial h}{\partial r} \right)^2 + \frac{1}{3} h^3 \frac{\partial^2 h}{\partial r^2} + v_n, & r > 0. \end{cases} \quad (4.4)$$

v_n models the blowing or suction out of the slot. We consider blowing or suction on an interval of size L starting at $r = r_0$. A suitable function is given by Roy et al. [12]

$$v_n = \begin{cases} A \sin \left[\frac{\pi (r - r_0)}{L} \right], & r_0 \leq r \leq r_0 + L, \\ 0 & r \text{ elsewhere.} \end{cases} \quad (4.5)$$

$A > 0$ represents the amplitude of the blowing. $A < 0$ is the amplitude of the suction. The slot is a porous circular disk on the solid substrate and in Figure 4.1 we plot a top view of the substrate.

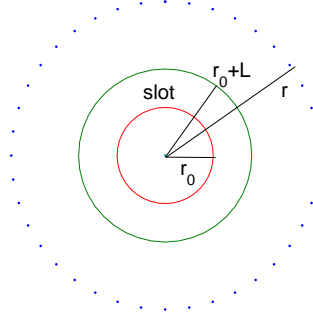


Fig. 4.1: Top view of the substrate.

In Figure 4.2 we plot the velocity profile v_n for both suction and injection. In the figures the position of the slot is indicated by the symbol *.

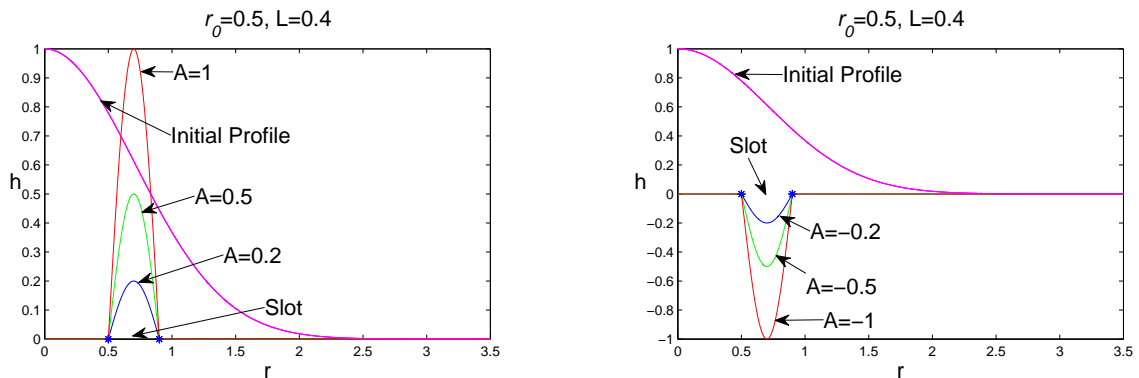


Fig. 4.2: Plot of v_n for different values of A and $L = 0.4$ where $r_0 = 0.5$.

The spreading of a liquid drop on a porous base has been investigated by Davis and Hocking [27, 28], while Sherman [7] has investigated the model on a non porous substrate. Mason and Momoniat [10] considered a group invariant solution for the axisymmetric spreading of a thin liquid drop under gravity only with suction or blowing at the horizontal base. However, the normal component at the base, v_n , was an unspecified function of the radial co-ordinate and time. The influence of slot injection/suction has been investigated by Momoniat and Mason [10, 13] and recently by Momoniat et al. [35] with gravity and surface tension being the driving forces. They obtain a non-linear fourth order partial differential equation. Momoniat et al. [35] have solved (4.4) using NDSolve in Mathematica.

In Figure 4.3 we plot the numerical solution admitted by equation (4.4) for varying magnitudes of injection, namely, $A = 0$, $A = 0.5$ and $A = 1$. $A = 0$ implies that $v_n = 0$, thus indicating that we have no suction/injection. The position of the slot is fixed at $r_0 = 0.5$ and the width of the slot is $L = 0.25$. When fluid is injected into the slot, we notice that the free surface profile is no longer smooth but has the formation of a ridge. The height of the ridges increase as we increase the amount of fluid being injected into the fluid. We also note that for the pseudospectral

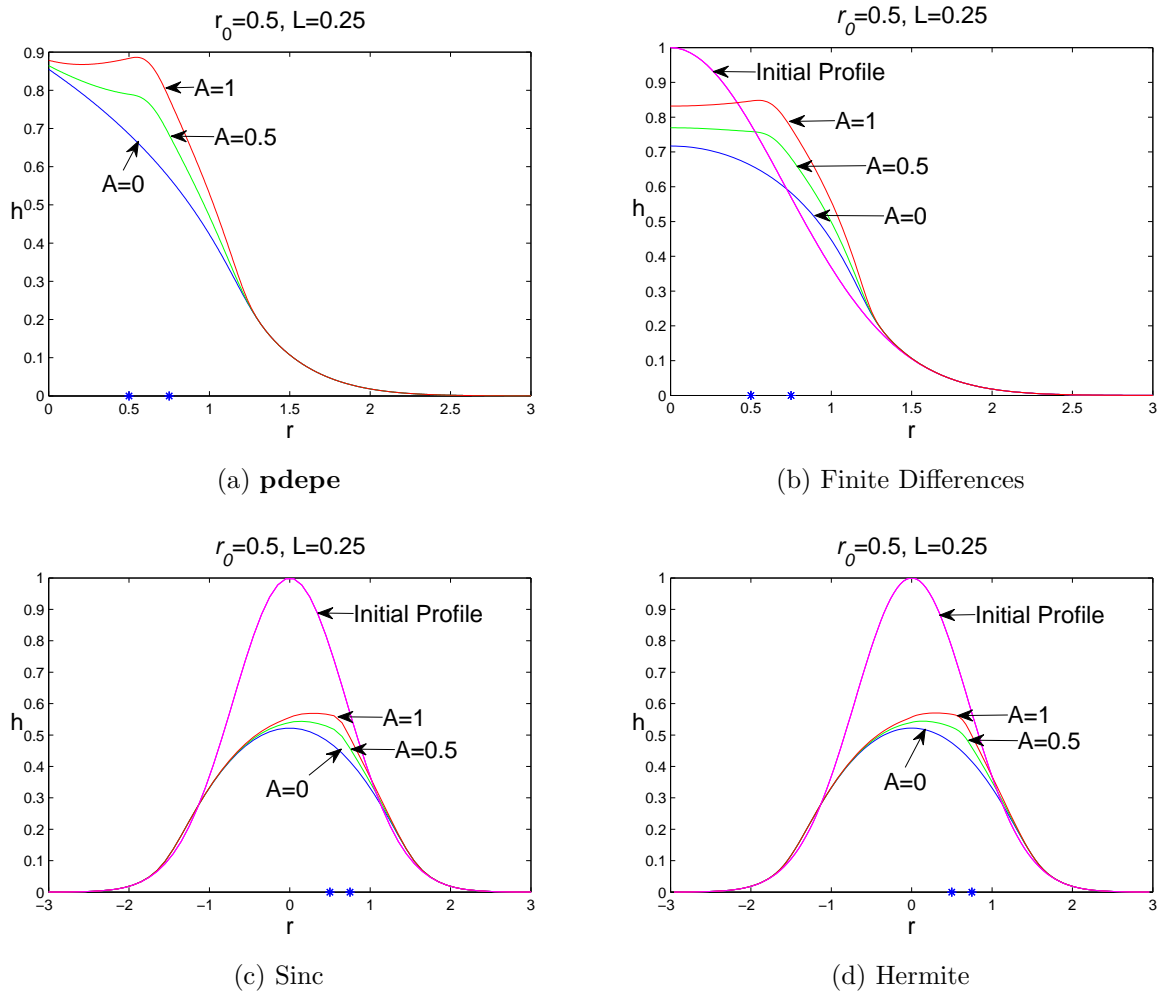


Fig. 4.3: Plot of the numerical solution of (4.4) at $r_0 = 0.5$ and $L = 0.25$ for varying magnitudes of injection where $A = 0$, $A = 0.5$ and $A = 1$.

methods, the height of the free surface profile falls down much faster as compared to the other two methods whilst the ridges are more prominent for the finite differences and **pdepe**.

In Figure 4.4 we plot the numerical solution admitted by equation (4.4) for varying magnitudes of suction, namely, $A = 0$, $A = -0.5$ and $A = -1$. The position of the slot is fixed at $r_0 = 0.5$ and the width of the slot is $L = 0.25$. We no longer have a smooth surface profile but the formation of a cavity when fluid is sucked out of the slot. We notice from Figure 4.4 that the depth of the cavities increase as we increase the magnitude of suction. We also note in Figure 4.4(a), the cavities

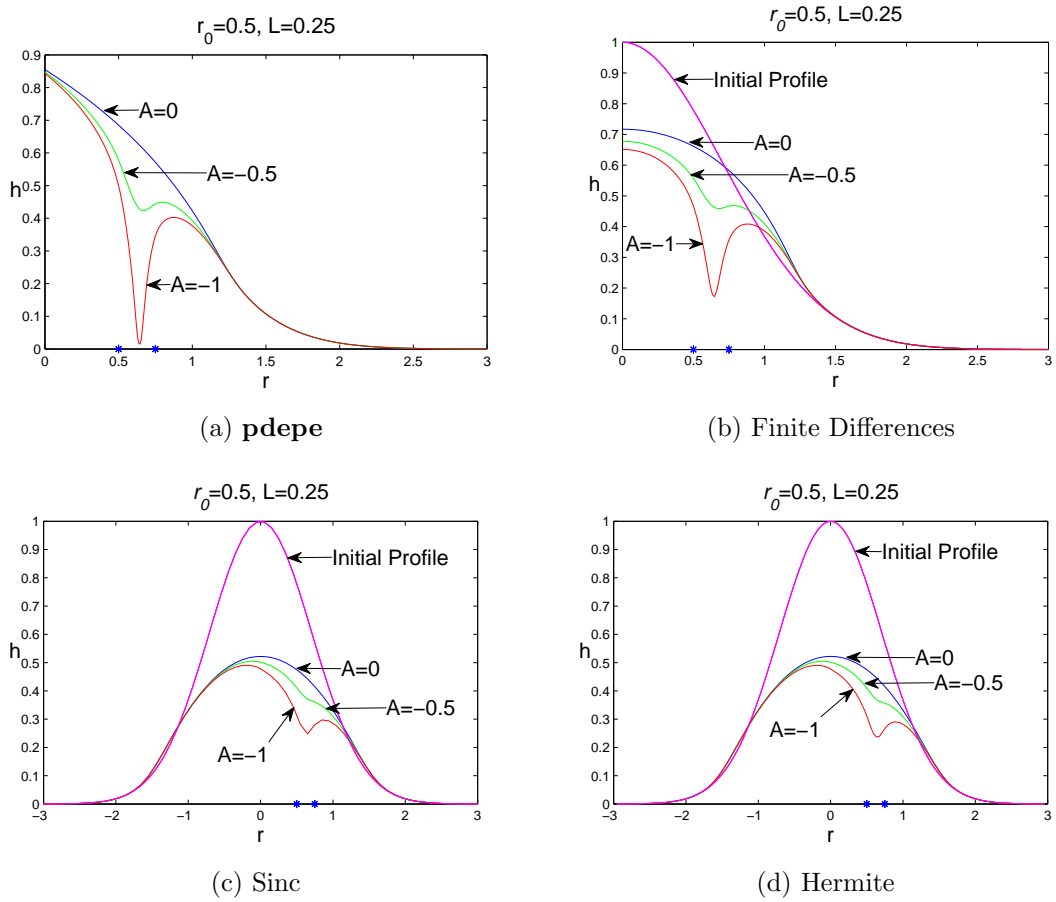


Fig. 4.4: Plot of the numerical solution of (4.4) at $r_0 = 0.5$ and $L = 0.25$ for varying magnitudes of suction where $A = 0$, $A = -0.5$ and $A = -1$.

have the greatest depth while in Figure 4.4(c) and Figure 4.4(d) the height of the free surface profile has fallen quite rapidly and the depth of the cavities are not as prominent as the other methods, although they are visible.

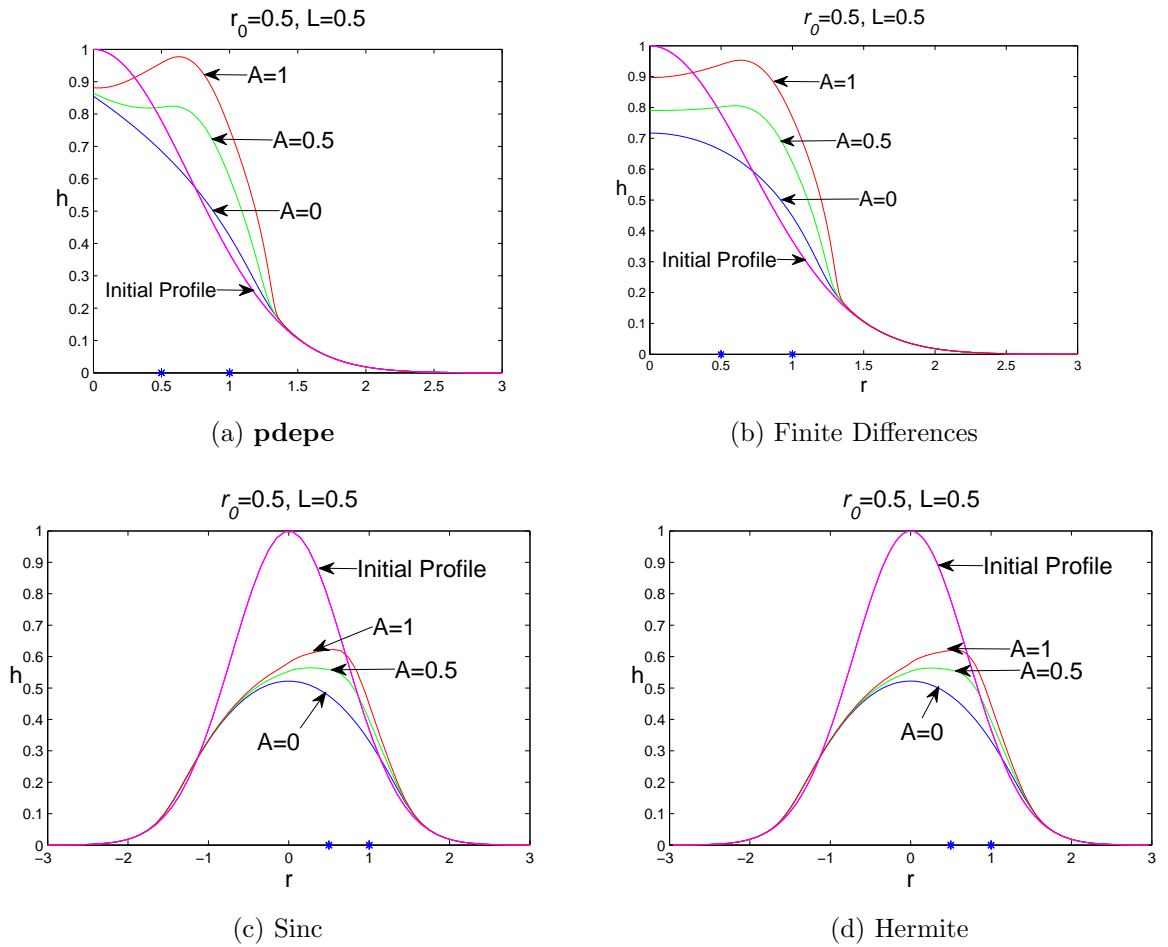


Fig. 4.5: Plot of the numerical solution of (4.4) at $r_0 = 0.5$ for varying magnitudes of injection where $A = 0$, $A = 0.5$ and $A = 1$. The width of the slot is changed to $L = 0.5$.

In Figure 4.5 and Figure 4.6 we examine the effect of increasing the slot width.

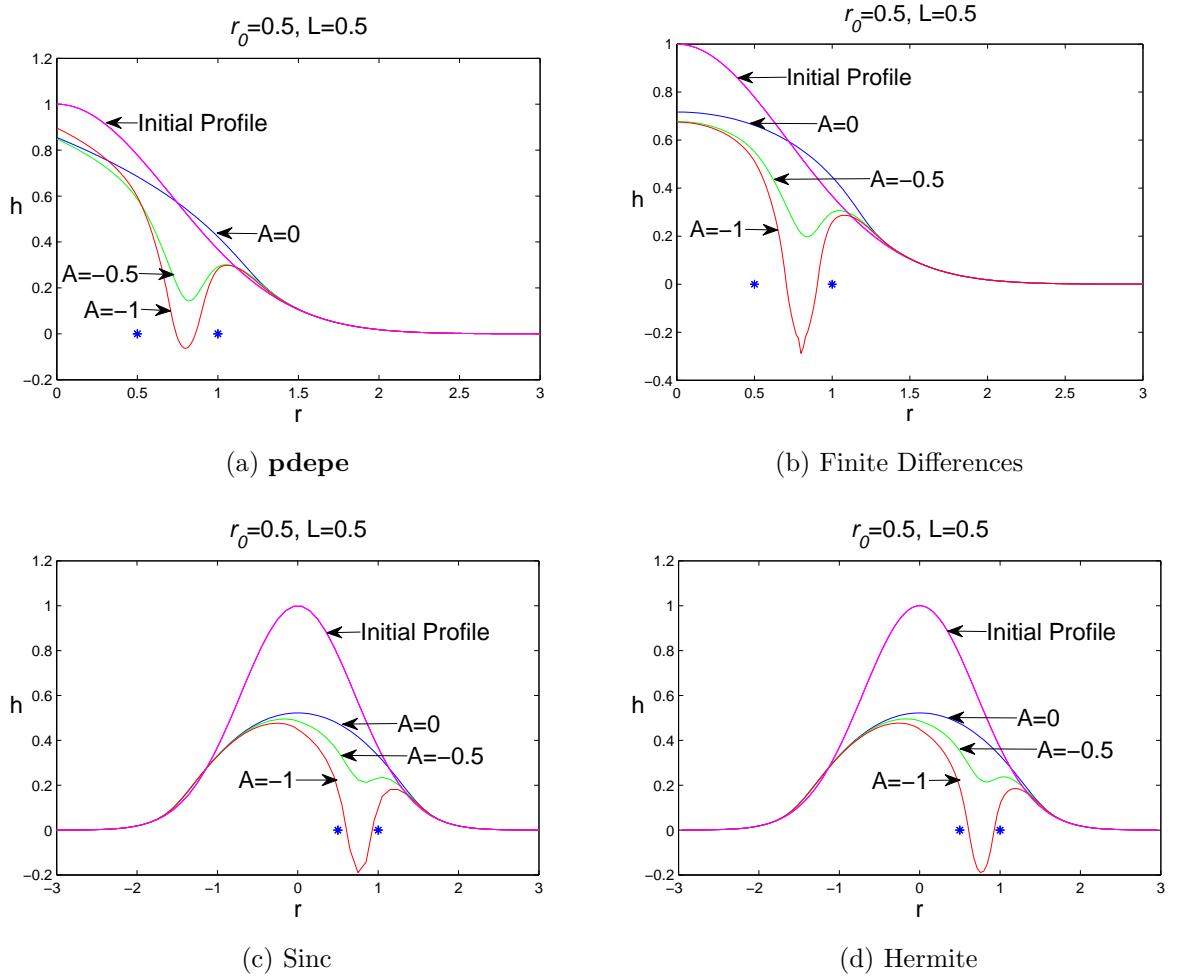


Fig. 4.6: Plot of the numerical solution of (4.1) at $r_0 = 0.5$ for varying magnitudes of suction where $A = 0$, $A = -0.5$ and $A = -1$. The width of the slot is changed to $L = 0.5$.

We increase the width of the slot from $L = 0.25$ to $L = 0.5$. We notice from Figure 4.5 that the amplitude of the ridges have increased and that they are even higher than the initial profile and that the cavities in Figure 4.6 have also increased in

magnitude. We also note in Figure 4.6 that for $A = -1$ the height of the free surface profile goes below zero signifying that all the fluid has been sucked through the slot.

In this chapter we have considered the effects of injection/suction on the free surface profile of the thin film when gravity alone is the driving force. Slot injection caused the formation of ridges while slot suction caused the formation of cavities on the free surface profile. As the effects of injection were increased, the ridges increased in magnitude. An increase in the magnitude of suction also resulted in an increase in the magnitude of the cavities. An increase in the width of the slot resulted in an increase of the height of the ridges and depth of the cavities. We also notice from the figures plotted that the Sinc and Hermite methods produced almost identical graphs, this is due to the fact that these methods have very similar convergence properties.

Chapter 5

SINGLE SLOT INJECTION/SUCTION WITH THE EFFECTS OF BOTH GRAVITY AND ROTATION

In this chapter we consider the effects of injection/suction on the free surface profile of the thin film when both gravity and rotation are the driving forces by employing the various numerical techniques discussed in chapter 3.

In this chapter the equation to be solved numerically is

$$\frac{\partial h}{\partial t} = \frac{1}{3r} \frac{\partial}{\partial r} \left(rh^3 \frac{\partial h}{\partial r} - \lambda r^2 h^3 \right) + v_n. \quad (5.1)$$

Once again there is a complication at $r = 0$ and by making the approximation as in chapter 4, the equation modeling the free surface profile is given as

$$\frac{\partial h}{\partial t} = \begin{cases} h^2 \left(\frac{\partial h}{\partial r} \right)^2 + \frac{2}{3} h^3 \frac{\partial^2 h}{\partial r^2} + \frac{2}{3} h^3 + rh^2 \frac{\partial h}{\partial r} + v_n, & r = 0, \\ \frac{1}{3} \frac{h^3}{r} \frac{\partial h}{\partial r} - h^2 \left(\frac{\partial h}{\partial r} \right)^2 + \frac{1}{3} h^3 \frac{\partial^2 h}{\partial r^2} + \frac{2}{3} + rh^2 \frac{\partial h}{\partial r} + v_n, & r > 0. \end{cases} \quad (5.2)$$

We firstly consider the case

$$v_n = 0. \quad (5.3)$$

In Figure 5.1 we plot the numerical solution of equation (5.2) for $v_n = 0$. The magnitude of rotation is varied where $\lambda = 0$, $\lambda = 0.5$ and $\lambda = 1$. When $\lambda = 0$ we

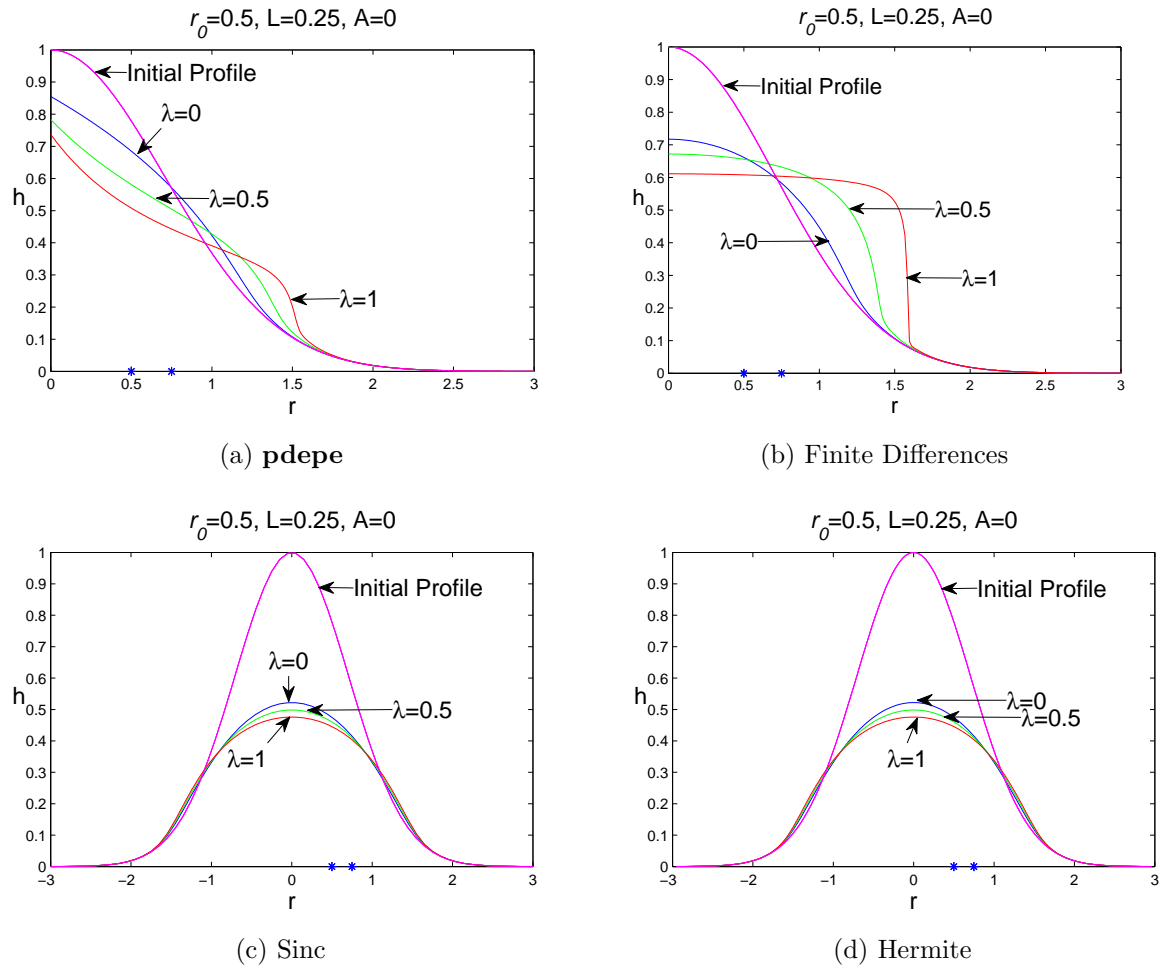


Fig. 5.1: Plot of the numerical solution of (5.2) for $v_n = 0$ and the magnitude of rotation is varied where $\lambda = 0$, $\lambda = 0.5$ and $\lambda = 1$.

have no rotation and gravity is the driving force. We notice from Figure 5.1 that when we have both rotation and gravity as the driving forces, the surface profile becomes flatter and decreases, however as we increase the effect of rotation we notice that the surface profile steepens and we have the formation of a breaking wave. The breaking wave is only visible in Figures 5.1(a) and 5.1(b) and not in

Figures 5.1(c) and 5.1(d). The reason for this is that the pseudospectral methods cannot integrate across the singularities, so it has actually smoothed out the discontinuities, and one of the shortcomings of the method is that it is inefficient in the presence of shocks, as can be seen in Figure 5.1.

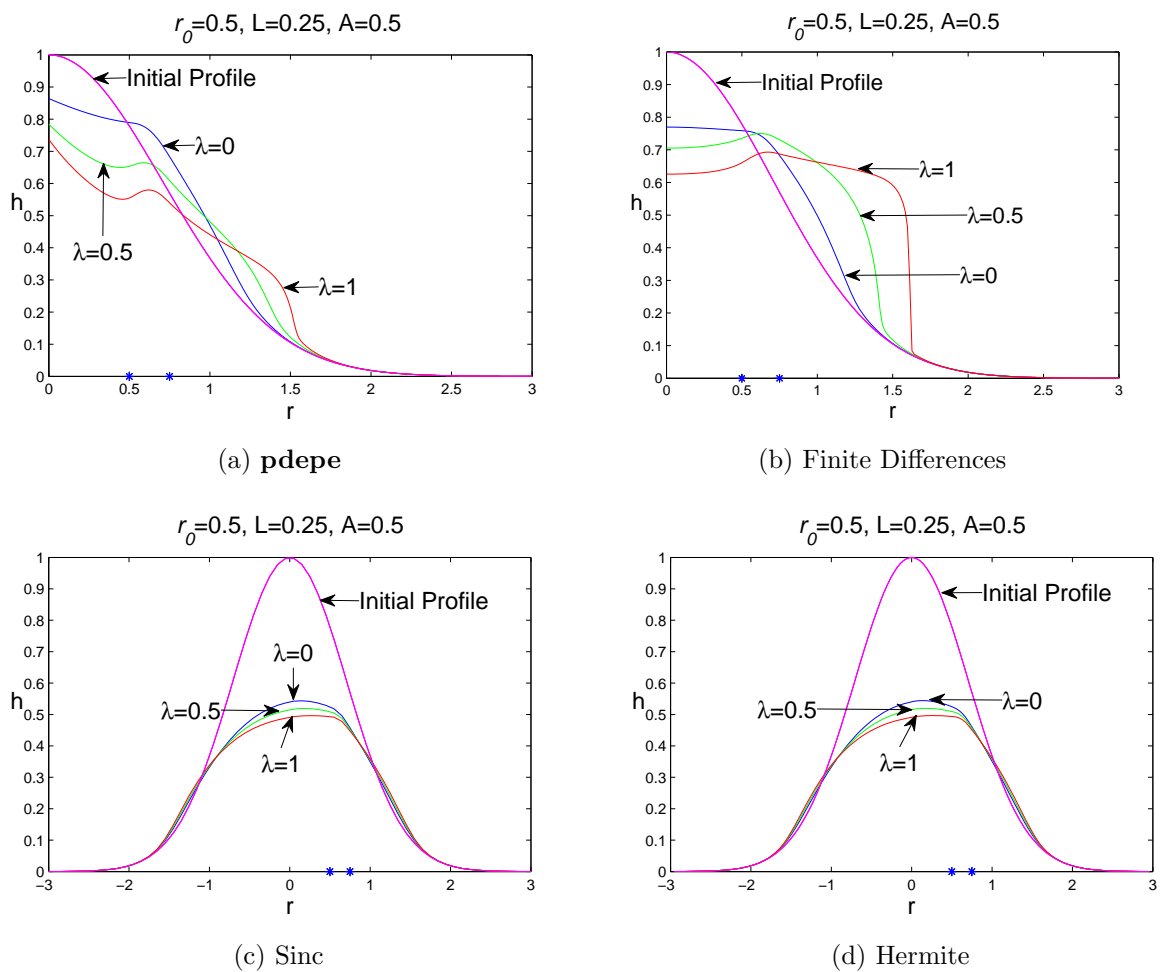


Fig. 5.2: Plot of the numerical solution of (5.2) where $r_0 = 0.5$, $L = 0.25$, $A = 0.5$. The magnitude of the rotation is varied where $\lambda = 0$, $\lambda = 0.5$ and $\lambda = 1$.

In Figure 5.2 and Figure 5.3 the surface profile is plotted for varying magnitudes of λ . The position of the slot is fixed at $r_0 = 0.5$ and the width of the slot is $L = 0.25$. The magnitude of injection is varied where $A = 0.5$ and $A = 1$. Rotation decreases the height of the surface profile. Once again, we notice as in

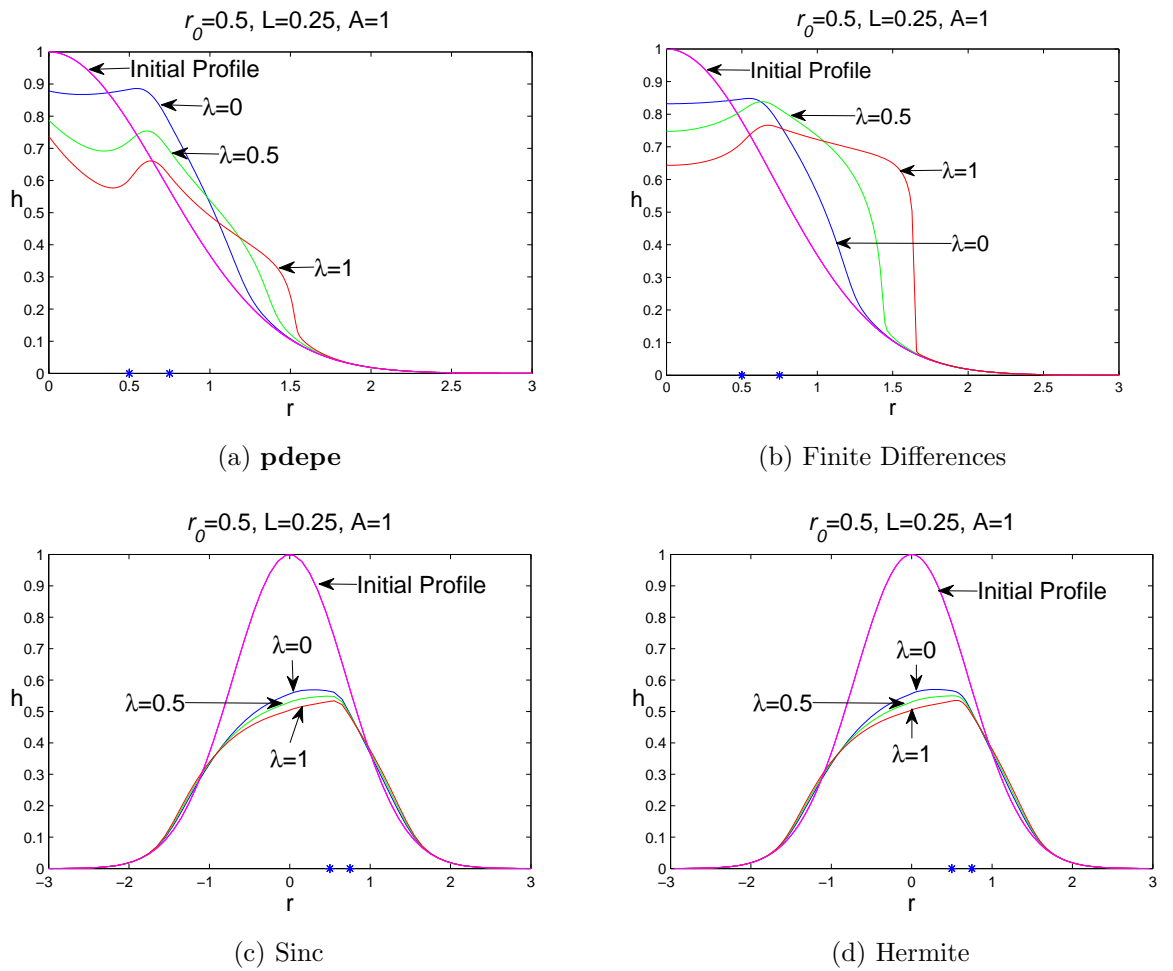


Fig. 5.3: Plot of the numerical solution of (5.2) where $r_0 = 0.5$, $L = 0.25$, $A = 1$. The magnitude of the rotation is varied where $\lambda = 0$, $\lambda = 0.5$ and $\lambda = 1$.

chapter 4, that increasing the magnitude of injection increases the height of the ridges on the free surface, however, the ridges are barely visible in Figures 5.2(c), 5.2(d), 5.3(c) and 5.3(d) for the pseudospectral methods. From Figure 5.3(b) one notices that the profile develops an infinite gradient for both $\lambda = 0.5$ and $\lambda = 1$.

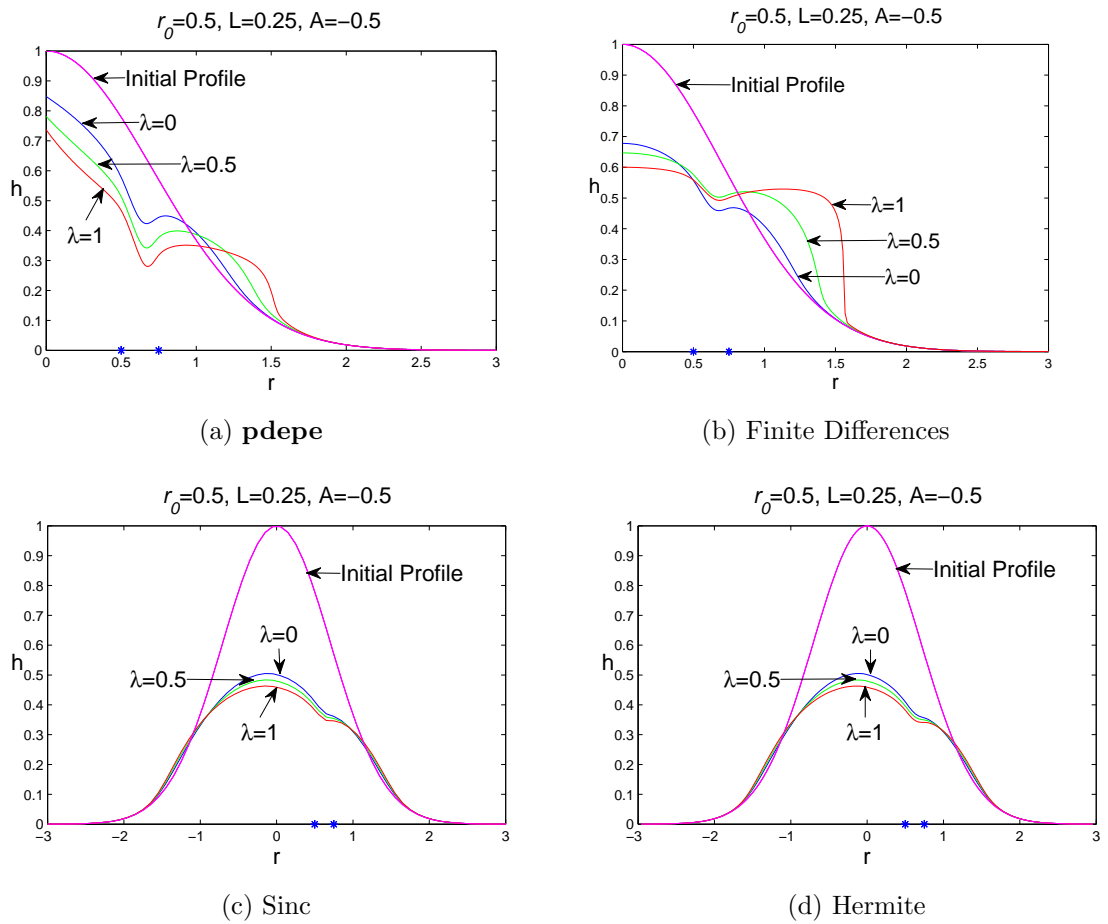


Fig. 5.4: Plot of the numerical solution of (5.2) where $r_0 = 0.5$, $L = 0.25$, $A = -0.5$. The magnitude of the rotation is varied where $\lambda = 0$, $\lambda = 0.5$ and $\lambda = 1$.

In Figure 5.4 and Figure 5.5 we fix the position of the slot at $r_0 = 0.5$ and the width of the slot to $L = 0.25$. The magnitude of suction is varied where $A = -0.5$ and $A = -1$. We plot the free surface profile for varying magnitudes of rotation. In both Figures 5.4 and 5.5 we note that an increase in the magnitude of rota-

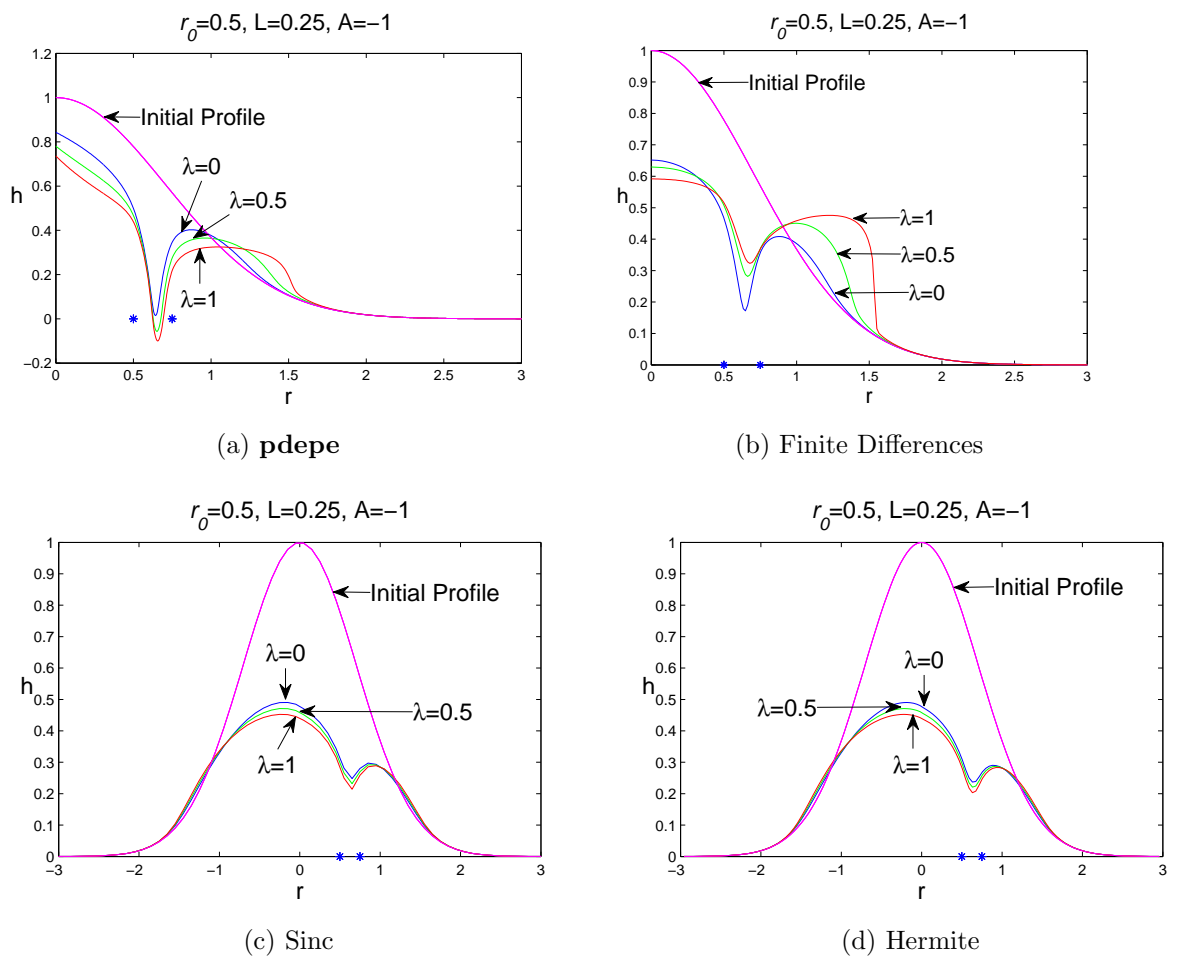


Fig. 5.5: Plot of the numerical solution of (5.2) where $r_0 = 0.5$, $L = 0.25$, $A = -1$. The magnitude of the rotation is varied where $\lambda = 0$, $\lambda = 0.5$ and $\lambda = 1$.

tion decreases the height of the surface profile. We also note as in chapter 4 that the greater the amount of the fluid being sucked out of the slot the greater the amplitude of the cavities. For $A = -1$ in Figure 5.5(a), we note that the surface profile goes below zero signifying that the all the fluid has been absorbed through the slot. We also have the formation of a breaking wave for $\lambda = 1$ for the finite

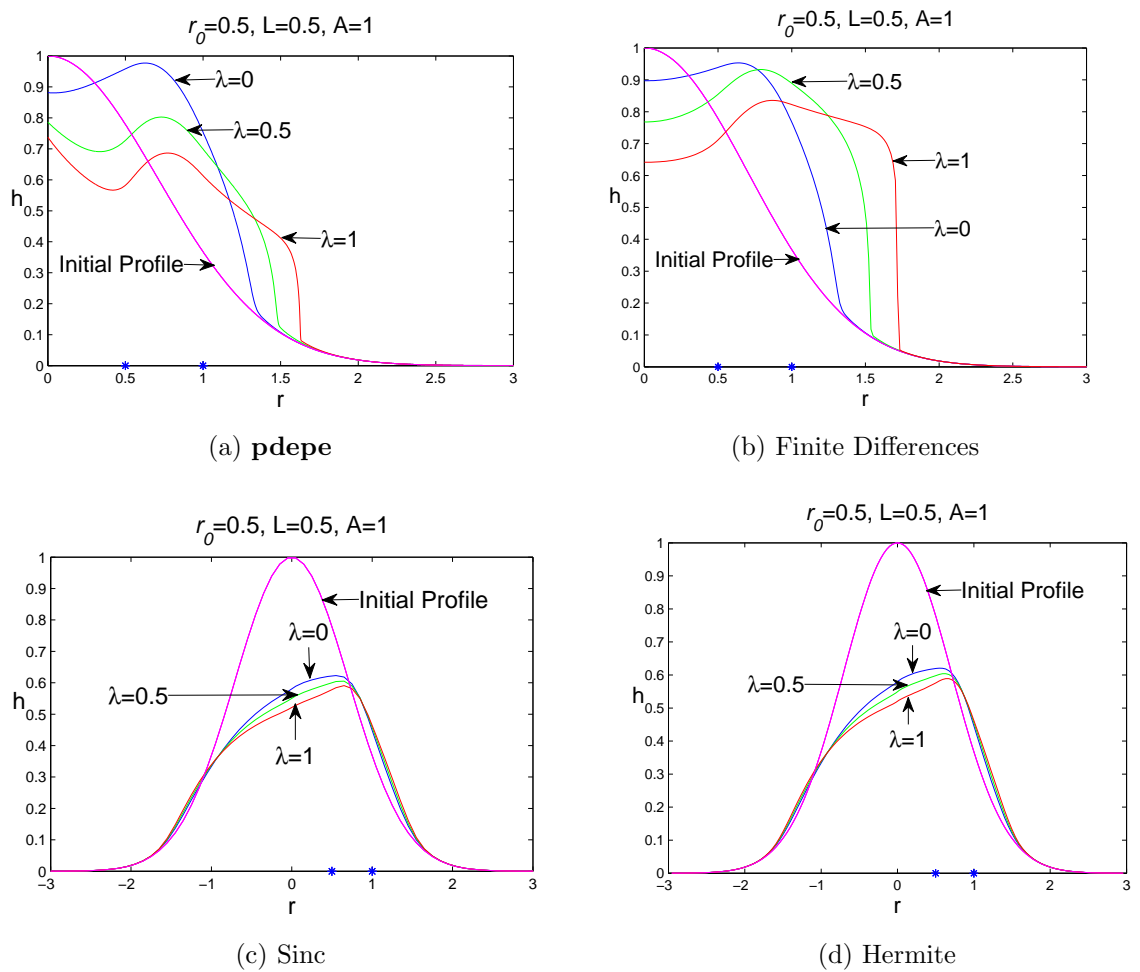


Fig. 5.6: Plot of the numerical solution of (5.2) where $r_0 = 0.5$, $A = 1$ and varying magnitudes of rotation. The width of the slot is changed to $L = 0.5$.

difference method and **pdepe**.

In Figure 5.6 and 5.7 we compare the effect of increasing the width of the slot from $L = 0.25$ to $L = 0.5$. We note that for both suction and injection, the amplitude of

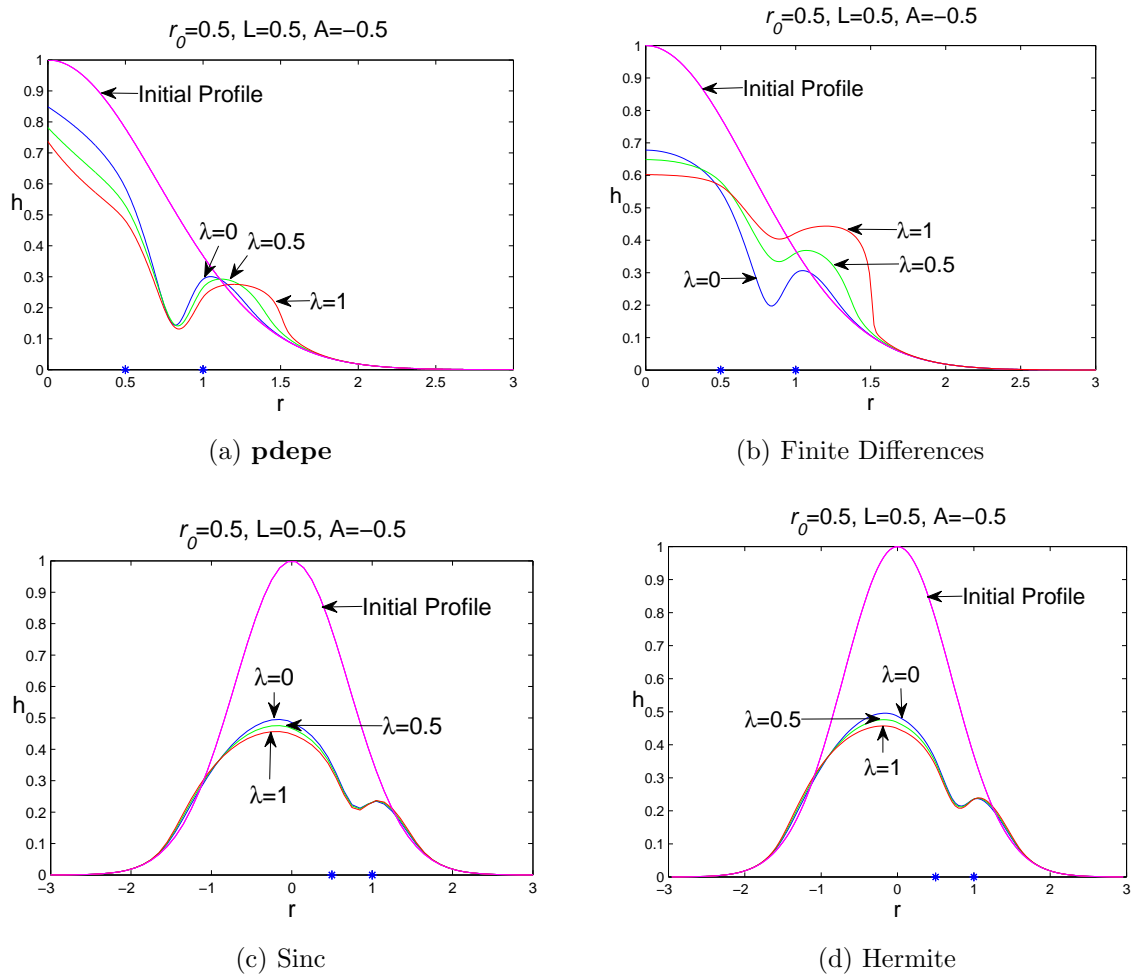


Fig. 5.7: Plot of the numerical solution of (5.2) where $r_0 = 0.5$, $A = -0.5$ and varying magnitudes of rotation. The width of the slot is changed to $L = 0.5$.

the cavities and ridges have increased. In 5.6(a) we have a breaking wave for $\lambda = 1$ while in 5.6(b) we have an infinite gradient for both $\lambda = 0.5$ and $\lambda = 1$. Once again we notice that the breaking wave phenomena is not present in the graphs from the pseudospectral methods.

From the work done in this chapter we can conclude that rotation increases the spreading of the thin film thus resulting in a decrease in the height of the free surface profile. Increasing the effects of rotation decreases the height of the free surface profile. By increasing the width of the slot, we observed an increased height of the ridges and depth of the cavities forming. We also notice that the pseudospectral methods, namely, Hermite and Sinc methods were inefficient in solving our problem. They actually smoothed out the discontinuities and we did not see the shocks that were present in the graphs from the other methods. Both the Hermite and Sinc methods produced similar graphs once again.

Chapter 6

SINGLE SLOT SUCTION WITH THE EFFECT OF ROTATION ONLY

In this chapter we consider the effects of slot suction on the free surface profile of the thin film when rotation alone is the driving force by employing the various numerical techniques discussed in chapter 3.

The equation which models the evolution of the free surface profile under the effect of rotation alone with slot injection/suction is given as

$$\frac{\partial h}{\partial t} = \frac{1}{3r} \frac{\partial}{\partial r} \left(-\lambda r^2 h^3 \right) + v_n, \quad (6.1)$$

When doing the computation for blowing we obtained many singularities and so we will not be considering it any further. The numerical method described by **pdepe** was the only method that was able to solve (6.1) while the other methods were inefficient and produced singularities.

We firstly consider the case

$$v_n = 0. \quad (6.2)$$

When fluid is not injected into the slot, we obtain the equation first derived by Emslie et al. [8]. Emslie showed that if we have an initial condition that is ever decreasing, we will have shocks developing, which are sharp jumps in the film thickness. The Lie group method has also been used to find a new implicit solution for rotation-driven spreading when there is no injection/suction [11].

In Figure 6.1 we plot the numerical solution of (6.1) for $v_n = 0$. The magnitude of rotation is varied where $\lambda = 0.1$, $\lambda = 0.5$ and $\lambda = 1$. We notice from Figure 6.1 that when rotation is the only driving force, the free surface profile does not decrease in height but remains at a constant height, however, the liquid actually thins and does not spread. As we increase the effect of rotation we notice that the surface profile steepens and we have the formation of a breaking wave.

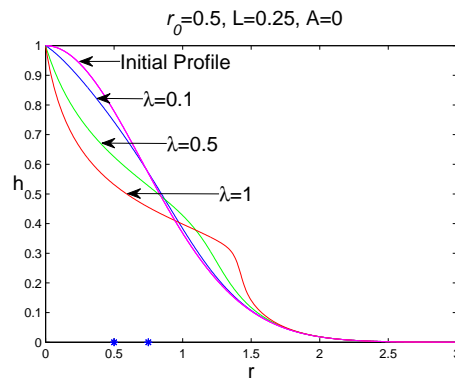


Fig. 6.1: Plot of the numerical solution of (6.1) for $v_n = 0$ and the magnitude of rotation is varied where $\lambda = 0.1$, $\lambda = 0.5$ and $\lambda = 1$.

In Figure 6.2 the surface profile is plotted for varying magnitudes of λ . The position of the slot is fixed at $r_0 = 0.5$ and the width of the slot is $L = 0.25$. The magnitude of suction is varied where $A = -0.5$ and $A = -1$. We note that suction does not affect the height of the free surface profile at the center of the fluid and as we increase the magnitude of suction, the depth of the cavities increases. For $\lambda = 1$ we have the formation of a breaking wave. For $A = -1$ the profile goes below zero signifying that the fluid has been sucked through the slot.

In Figure 6.3 we compare the effect of increasing the width of the slot from $L = 0.25$ to $L = 0.5$. The surface profile is plotted for varying magnitudes of λ . The posi-

tion of the slot is fixed at $r_0 = 0$. We note that the amplitude of the cavities have increased due to an increase in the amount of fluid being sucked out of the fluid as a result of a wider slot.

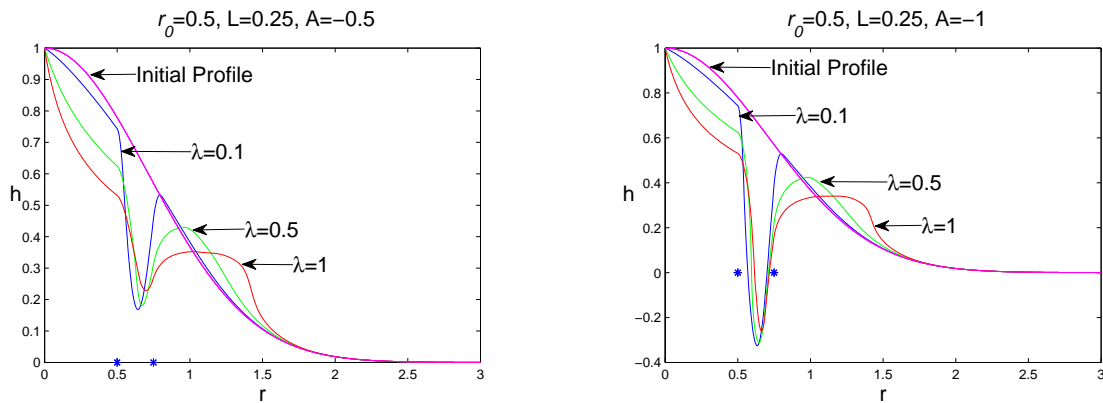


Fig. 6.2: Plot of the numerical solution of (6.1) where $r_0 = 0.5$, $L = 0.25$, $A = -0.5$ and $A = -1$. The magnitude of the rotation is varied where $\lambda = 0.1$, $\lambda = 0.5$ and $\lambda = 1$.

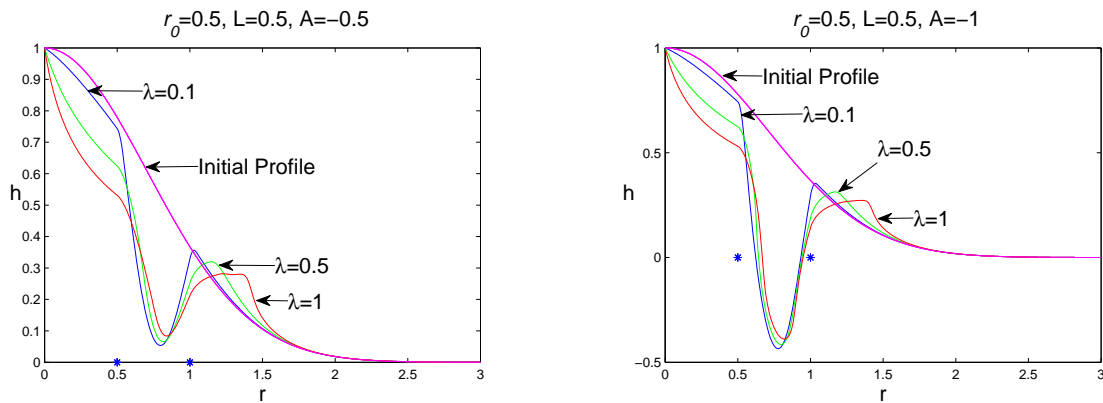


Fig. 6.3: Plot of the numerical solution of (6.1) where $r_0 = 0.5$, $A = -0.5$ and $A = -1$ and varying magnitudes of rotation. The width of the slot is changed to $L = 0.5$.

We would like to consider the effect that the slot has on the wave breaking process. We will not be using the numerical techniques discussed in chapter 3 as the integration failed and singularities occurred due to the position of the slot competing with the satisfaction of the boundary conditions. If we let $\lambda = 1$ in equation (6.1), where the wave breaking occurred, we obtain a first order quasi-linear partial differential equation

$$\begin{aligned}\frac{\partial h}{\partial t} + \frac{1}{3r} \frac{\partial}{\partial r} (r^2 h^3) - v_n &= 0, \\ \frac{\partial h}{\partial t} + r h^2 \frac{\partial h}{\partial r} + \frac{2}{3} h^3 - v_n &= 0, \\ \frac{\partial h}{\partial t} + r h^2 \frac{\partial h}{\partial r} &= -\frac{2}{3} h^3 + v_n.\end{aligned}\tag{6.3}$$

The problem is formulated as a Cauchy initial value problem. In 3-dimensional space (r, t, h) , we let σ denote the parameter along the initial curve

$$h(\sigma, 0) = \text{Exp}(-\sigma^2),\tag{6.4}$$

and let s denote the parameter along the characteristic curve. The

$$t = t(\sigma, s) \quad r = r(\sigma, s) \quad h = h(\sigma, s),\tag{6.5}$$

where h is a different function of (σ, s) then it was of (r, t) . The initial conditions at $s = 0$ are

$$t(\sigma, 0) = 0 \quad r(\sigma, 0) = \sigma \quad h(\sigma, 0) = \text{Exp}(-\sigma^2).\tag{6.6}$$

The differential equations of the characteristic curves are

$$\frac{d t}{d s} = 1,\tag{6.7}$$

$$\frac{d r}{d s} = r h^2,\tag{6.8}$$

$$\frac{d h}{d s} = -\frac{2}{3} h^3 + v_n.\tag{6.9}$$

We cannot find an analytic solution as equation (6.9) cannot be integrated. We solve the differential equations (6.7)-(6.9) numerically subject to initial conditions (6.6) by using NDSolve in MATHEMATICA. We firstly consider the case

$$v_n = 0. \quad (6.10)$$

When fluid is not injected into the slot, we obtain the equation first derived by Emslie et al. [8]. Emslie showed that if we have an initial condition that is ever decreasing, we will have shocks developing.

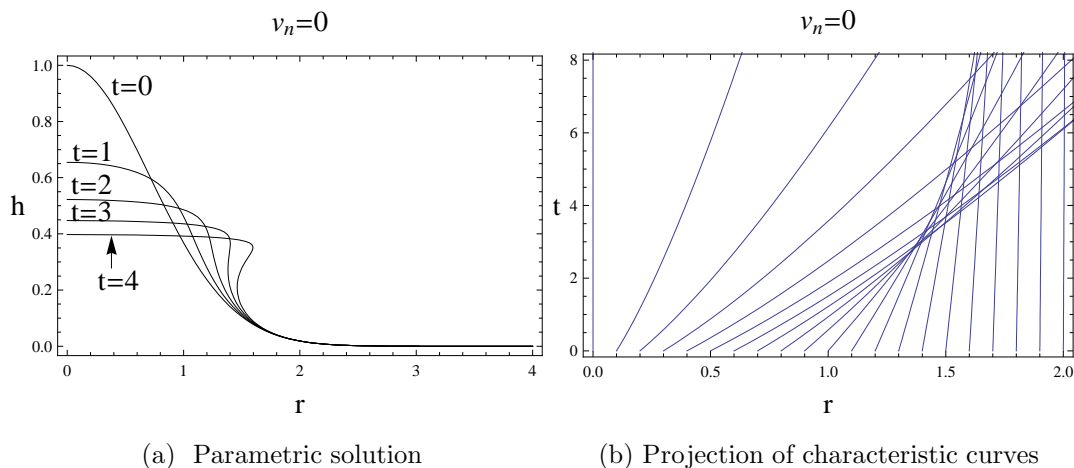


Fig. 6.4: Parametric solution for $t=0,1,2,3,4$ and projection of the characteristic curves on the (r,t) -plane for $v_n = 0$.

In Figure 6.4 we plot the numerical solution for $v_n = 0$. The graph of h against r is plotted for a range of t values as well as the projection of the characteristic curves on the (r,t) -plane. We notice that the surface profile flattens and decreases and eventually steepens and has the formation of a breaking wave. The breaking wave is illustrated in Figure 6.4(b) where the characteristic curves emanating from

the r -axis intersect and the minimum point on the envelope represents the radial position and time when the surface profile first breaks.

In Figure 6.5 we determine the effect that the slot width has on the formation of the breaking wave. The free surface profile is plotted at varying times. The position of the slot is fixed at $r_0 = 0.5$ and $A = -0.4$. The slot width is varied where $L = 0.25$, $L = 0.5$, $L = 0.8$ and $L = 1$. In Figure 6.5, we notice that the

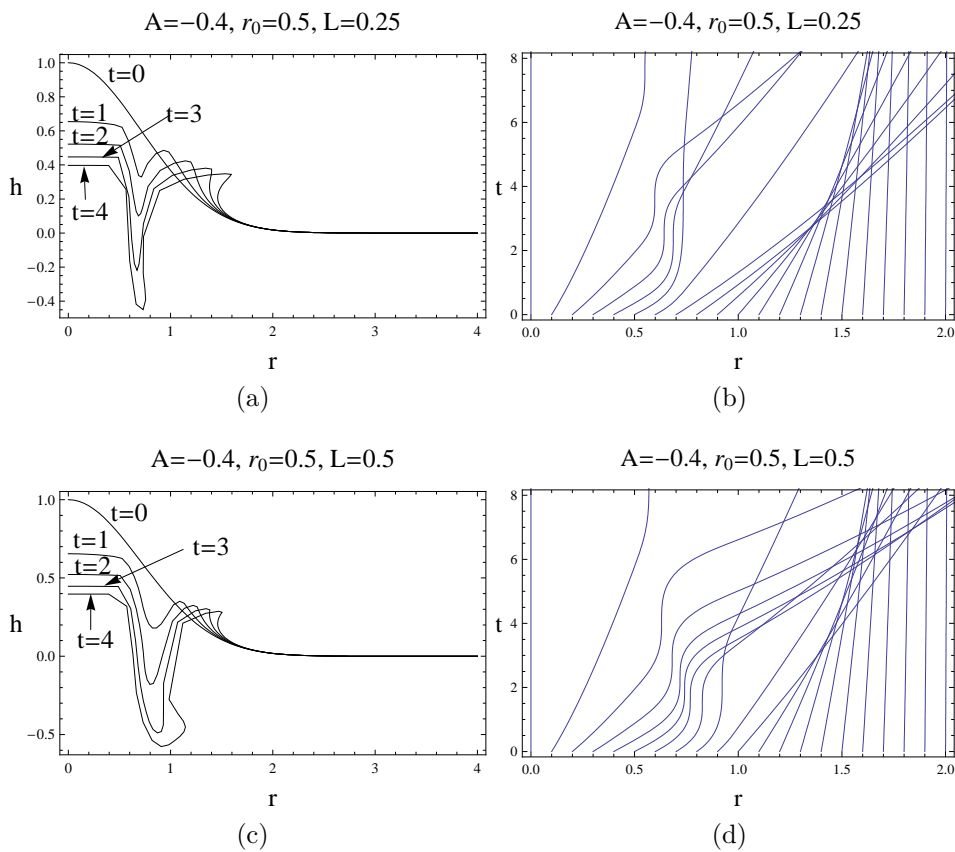


Fig. 6.5: Parametric solution and characteristic projection for varying slot widths.

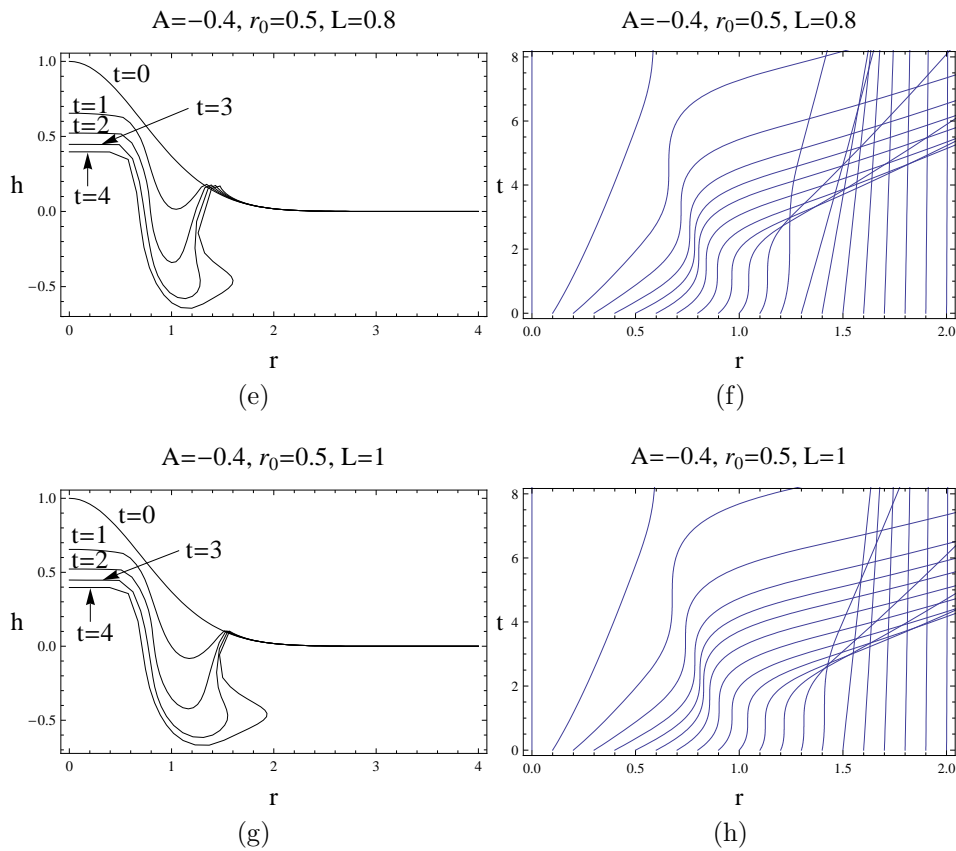


Fig. 6.5: *Parametric solution and characteristic projection for varying slot widths (cont).*

wave begins to break at time, $t = 3$. We also notice from the graphs of h plotted against r that as we increase the slot width, we increase the volume of fluid being sucked out through the slot, thus preventing the sharp jumps from forming in the free surface profile. This is further illustrated in the projection of the characteristic curves. From the graphs of the characteristic curves we notice wavy lines and straight lines so as to distinguish two types of behaviors. The wavy lines represent the surface profile before and during suction while the straight lines represent the

surface profile beyond the slot width. When the lines intersect it represents the breaking process of the surface profile, however in the case of the slot and slot position this signifies a mathematical breaking as the graphs goes below the zero axis. We also notice that in Figures 6.5(f) and 6.5(h) that at the end of the slot the lines are parallel and do not intersect signifying that we no longer have a multivalued wave and the wave does not break, which corresponds with the graphs of h plotted against r . Thus by increasing the slot width we can prevent the wave from breaking.

In Figure 6.6 we determine the effect that the magnitude of suction has on the breaking process of the free surface profile. The free surface profile is plotted at varying times. The position of the slot is fixed at $r_0 = 0.5$ and the width of the slot to $L = 0.25$. We compare the suction of $A = -0.2$ with that of $A = -0.4$. In Figure 6.6 it is clear that the magnitude of suction does not hamper or cause the breaking wave to develop earlier, however it does affect the depth of the cavities

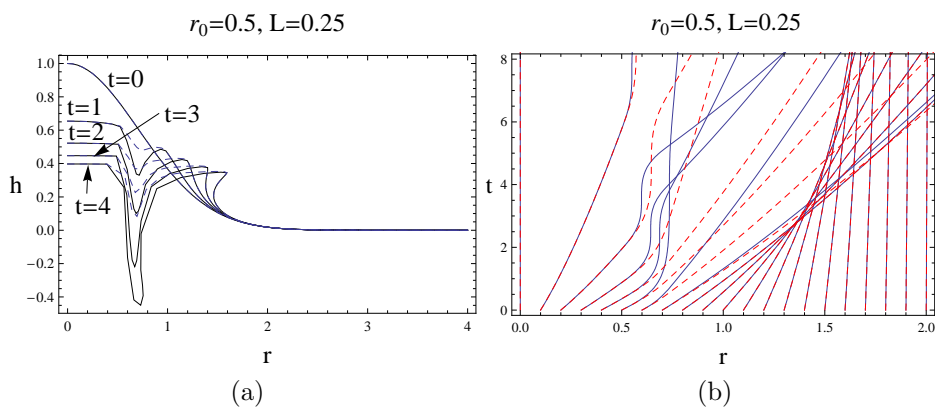


Fig. 6.6: Parametric solution and characteristic projection comparing slot magnitude $A = -0.4$ with $A = -0.2$ (---).

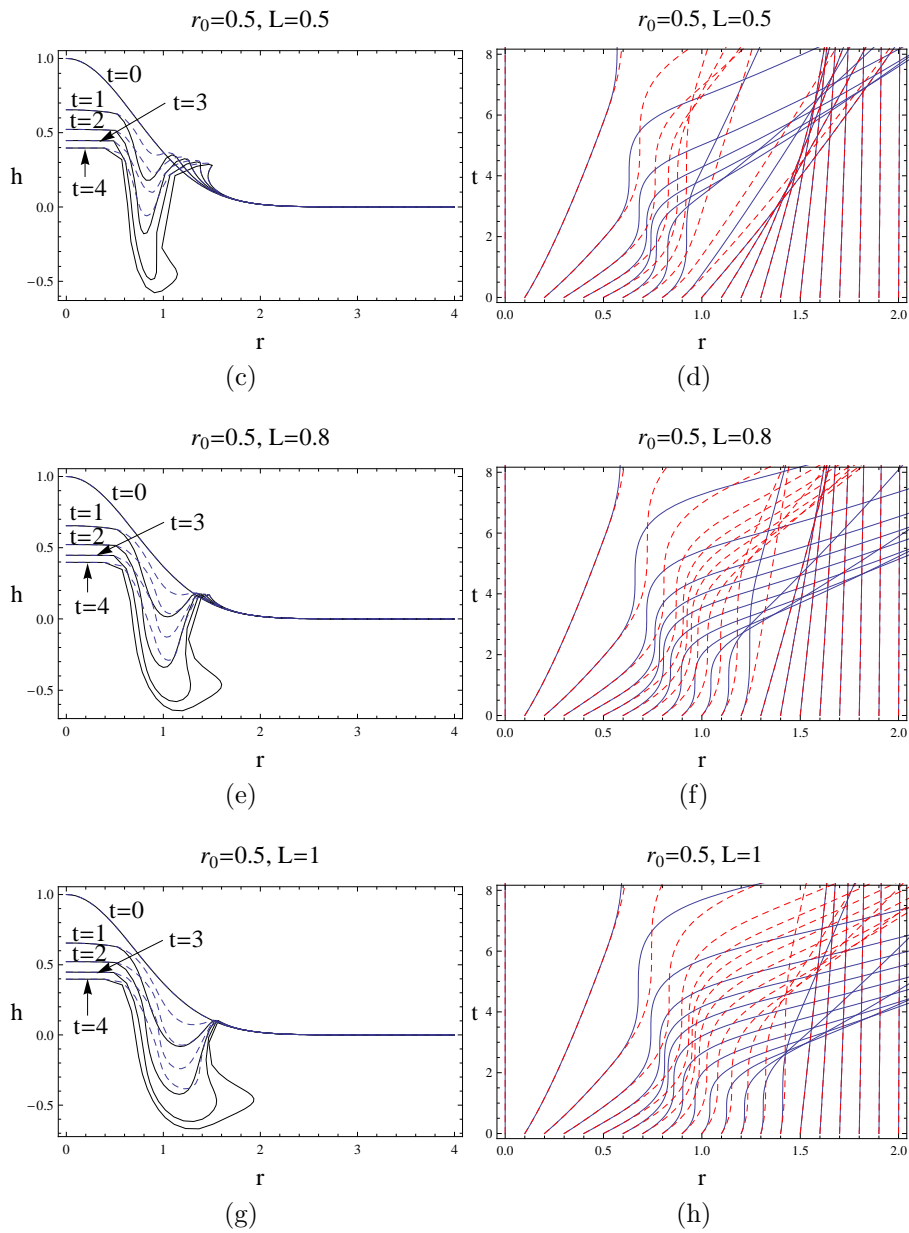


Fig. 6.6: Parametric solution and characteristic projection comparing slot magnitude $A = -0.4$ with $A = -0.2$ (---) (cont).

forming on the free surface profile. Increasing/decreasing the magnitude of suction increases/decreases the depth of the cavities. This is further illustrated when we project the characteristic curves on the $(r-t)$ plane. We notice that only the wavy lines differ signifying the behavior of the fluid within the slot. Beyond the slot we cannot differentiate between the two graphs as they overlap thus illustrating that varying the magnitude of suction does not affect the breaking process of the free surface profile.

In Figure 6.7 we determine the effect that the position of the slot has on the development of the breaking wave. The magnitude of suction is fixed at $A = -0.2$, and the slot width at $L = 0.25$. The position of the slot is varied where $r_0 = 0.5$, $r_0 = 0.8$ and $r_0 = 1.2$. We plot the graph of h against r as well as the characteristic projections on the $(r-t)$ -plane. Once again we notice that sharp jumps appear in the free surface profile at time $t = 3$. In Figure 6.7 we notice that as we move

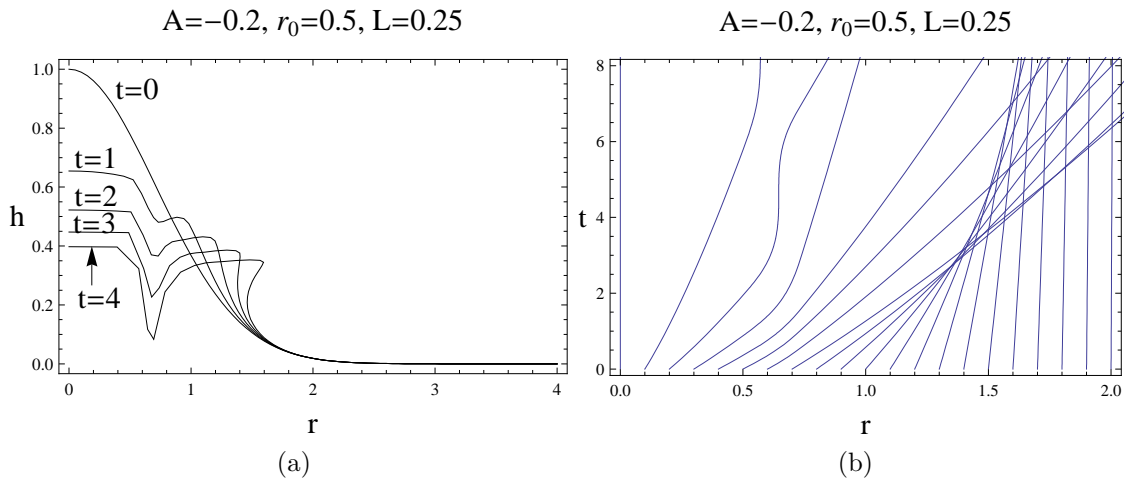


Fig. 6.7: Parametric solution and characteristic projection comparing slot position.

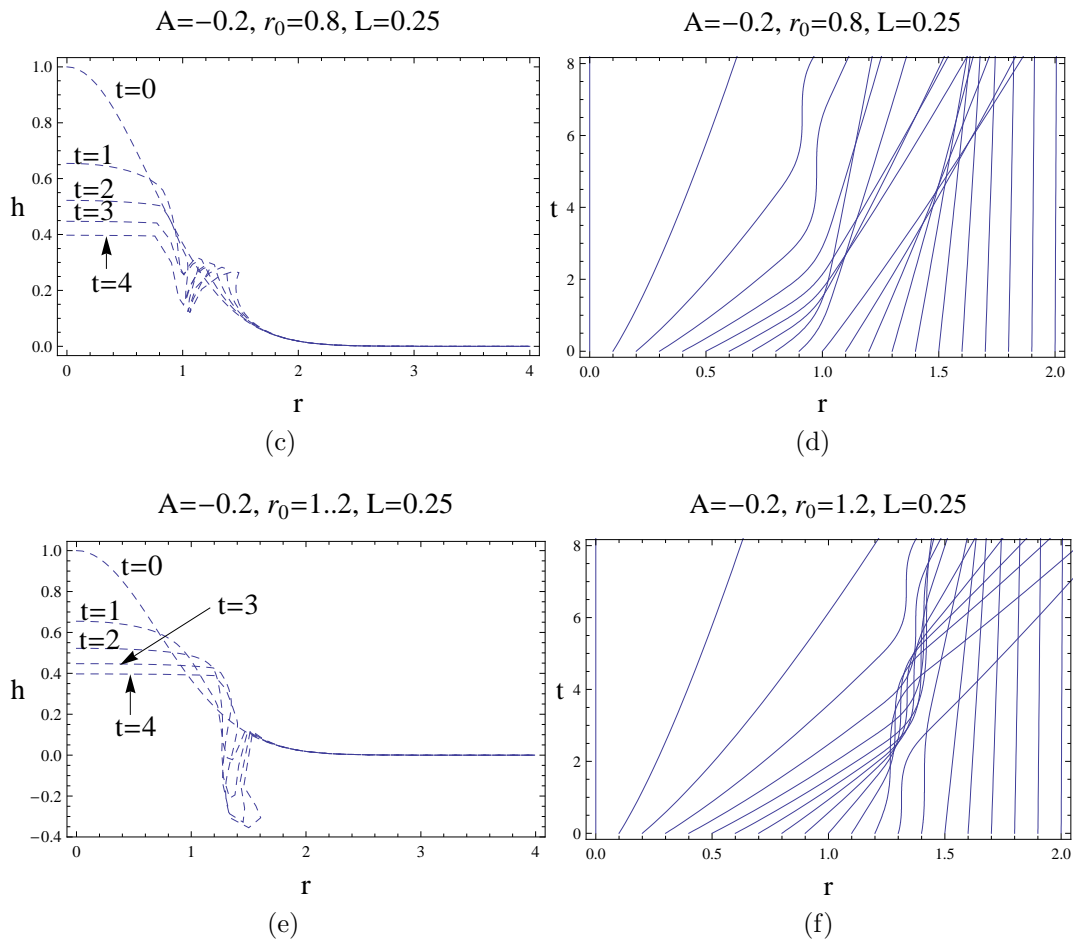


Fig. 6.7: Parametric solution and characteristic projection comparing slot positions (cont).

the slot further away from the center of the free surface profile, we have less film falling over and eventually we prevent the sharp jumps from forming. This is further illustrated if we look at the projections of the characteristic curves. In Figure 6.7(b) and Figure 6.7(d) we see that beyond the slot position the lines intersect indicating that the wave is still breaking, however in 6.7(f) we note that beyond the slot position the lines are parallel which signifies that we do not have a

breaking wave. The breaking of the wave that occurs in 6.7(f) at position $r = 1.3$ is a mathematical breaking as the graph has gone below the zero axis.

In this chapter we have considered the effects of the slot on the breaking process on the free surface profile. The graphs of h against r were plotted as well as the characteristic projections on the (r-t)-plane to further illustrate the effects. The width of the slot and the position of the slot were key influences in preventing a breaking wave from forming on the free surface profile, while the magnitude of suction did not affect the breaking process. The magnitude of suction affected the cavities forming on the free surface with an increase in the depth of the cavities as the suction was increased. Concluding remarks are made in the next chapter.

Chapter 7

CONCLUSION

In this dissertation, we have investigated the influence of slot injection/suction on the spreading of the thin axisymmetric film under gravity, rotation, and gravity coupled with rotation. We have used numerical techniques to investigate this spreading and compared the various techniques used in solving our problem.

We have used lubrication theory to derive the equation for the free surface profile of the film height. In lubrication theory the characteristic thickness, H , is assumed to be much smaller than the characteristic length of the film L_c :

$$\frac{H}{L_c} \ll 1.$$

In addition the assumption is also made that

$$Re \frac{H}{L_c} \ll 1,$$

where $Re = UL/\nu$ is the Reynolds number of the flow.

A normal v_n was induced at the surface of the disk. v_n modeled the blowing or suction out of the slot. A suitable function for v_n was given as follows

$$v_n = \begin{cases} A \sin \left[\frac{\pi(r - r_0)}{L} \right], & r_0 \leq r \leq r_0 + L, \\ 0 & r \text{ elsewhere.} \end{cases} \quad (7.1)$$

The amplitude of blowing was represented by $A > 0$ and the amplitude of suction was represented by $A < 0$.

We note that we have equivalent results for the effect of slot injection/suction when gravity is the only driving force, rotation is the only force and when we have gravity coupled with rotation. As injection is increased so to are the heights of the ridges. Increasing the effect of suction increases the depth of cavities. However rotation decreases the height of the free surface profile as compared to the effects of gravity alone. When rotation is coupled with gravity we also have deeper cavities and higher ridges forming as compared to the effects of gravity alone. As we increase the effects of rotation, we have the formation of a breaking wave for both slot injection and suction. Manipulating the width of the slot, does not affect the height at the center of the free surface profile but it does affect the amount of fluid being injected into or sucked out through the slot.

With regards to the numerical techniques used, **pdepe** was the most efficient in solving our problem while the pseudospectral methods were inefficient when rotation was coupled with gravity. The pseudospectral methods had smoothed out the discontinuities and we did not see the shocks developing in the free surface profile. The Sinc and Hermite pseudospectral methods produced almost identical graphs as they have similar convergence properties.

By using NDSolve in Mathematica we plotted the graphs of h against r for a range of t values as well as the projection of the characteristic curves on the $(r-t)$ -plane to determine the effect that the slot has on the wave breaking process when rotation is the only driving force coupled with suction. We find that either increasing the width of the slot or moving the position of the slot further from the center of the liquid film, we can hamper the formation of a breaking wave and even prevent the folding over of the wave that we seen when rotation was coupled with gravity. The magnitude of suction did not affect the wave breaking process.

Future work entails the use of multiple slots, as well as the inclusion of surface

tension with gravity and rotation and an extension to non-Newtonian fluids.

BIBLIOGRAPHY

- [1] E. Momoniat and D.P. Mason, Investigation of the effect of the Coriolis force on a thin liquid film on a rotating disk, *Int. J. Non-Linear Mech.*, **33** (6) (1998), 1069-1088
- [2] R. P. Gillespie, *Integration*, 6th edition. Oliver and Boyd, Edinburgh, 1959, 113–116.
- [3] J. H. Hwang and F. Ma, On the flow of a thin liquid film over a rough rotating disk, *J. Appl. Phys.*, **66** (1989) 388–394.
- [4] D. Meyerhofer, Characteristics of resist films produced by spinning, *J. Appl. Phys.*, **49** (1978), 3993
- [5] P.C. Sukanek, Spin Coating, *J. Imaging Technol*, **11** (1985), 184
- [6] B. Reisfeld, S. G. Bankoff and S. H. Davis, The dynamics and stability of thin liquid films during spin coating, *J. Appl. Phys.*, **70** (10) (1991) 5258–5266.
- [7] F. S. Sherman, *Viscous Flow*, McGraw-Hill, New-York, 1990.
- [8] A.G. Emslie, F.T. Bonner, L.G. Peck, Flow of a viscous liquid on a rotating disk, *J. Appl. Phys.*, **29** (5) (1958), 858-862
- [9] A. Acrivos, M.G. Shah, E.E. Petersen, On the flow of a non-Newtonian liquid on a rotating disk, *J. Appl. Phys.*, **31** (1960), 963-968

-
- [10] D. P. Mason and E. Momoniat, Axisymmetric spreading of a thin liquid drop with suction or blowing at the horizontal base, *Int. J. Non-Linear Mech.* **39** (2004) 1013–1026.
- [11] E. Momoniat and T. G. Myers, A new solution for rotation-driven spreading of a thin fluid film, *Int. J. Non-Linear Mech.* **41** (2006) 192–199.
- [12] S. Roy, P. Datta, R. Ravindran and E. Momoniat, Non-Uniform Multiple Slot injection (Suction) on a forced flow over a slender cylinder, *Int. J. Heat and Mass Transfer*, **50** (2007) 3190–3194.
- [13] E. Momoniat and D. P. Mason, Spreading of a thin film with suction or blowing including surface tension effects, *Comp. Math. Appl.*, **53** (2007) 198–208.
- [14] S. Middleman, *Modelling Axisymmetric Flows*, Academic Press, New York, 1995.
- [15] T. G. Myers and J. P. F. Charpin, The effect of the Coriolis force on axisymmetric rotating thin film flows *Int. J. Non-linear Mech.*, **36** (2000) 629–635.
- [16] T. G. Myers, Thin films with high surface tension, *SIAM Rev.*, **40** (1998) 441–462.
- [17] L. M. Hocking, Rival contact-angle models and the spreading of drops, *J. Fluid Mech.* **239** (1992) 671–681.
- [18] S. B. G. O’Brien and L. W. Schwartz, Thin Film Flows: Theory and Modeling, *Encyclopedia of Surface and Colloid Science* (2006) 6304–6317. <http://www.informaworld.com/10.1081/E-ESCS-120000885>.
- [19] E. B. Dussan V, The moving contact line: the slip boundary condition, *J. Fluid Mech.* **77** (1976) 665.

-
- [20] P. G. de Gennes, Wetting: statics and dynamics, *Rev. Mod. Phys.* **57** (1985) 827-863.
- [21] L. F. Shampine and M. W. Reichelt, The MATLAB ODE Suite, *SIAM J. Sci. Comput.* **18** (1) (1997) 1-22.
- [22] B. Fornberg, *A Practical Guide to Pseudospectral Methods*, Cambridge, New York: Cambridge University Press, 1996.
- [23] J. P. Boyd, *Chebyshev and Fourier Spectral Methods*, 2nd ed., Dover, New York, 2000.
- [24] D. J. Acheson, *Elementary fluid dynamics*, Clarendon Press, Oxford, 1990.
- [25] L. N. Trefethen, *Spectral Methods in Matlab*, SIAM, Philadelphia, 2000.
- [26] C. Canuto, M. Y. Hussaini, A. Quarteroni, and T. Zang, *Spectral Methods in Fluid Dynamics*, Springer-Verlag, New York, 1988.
- [27] S. H. Davis and L. M. Hocking, Spreading and imbibitions of viscous liquid on a porous base, *Phys. Fluids.* **11** (1) (1999) 48-57.
- [28] S. H. Davis and L. M. Hocking, Spreading and imbibitions of viscous liquid on a porous base II, *Phys. Fluids.* **12** (7) (2000) 1646-1655.
- [29] J. A. C. Weidman and S. C. Reddy, A MATLAB Differentiation Matrix Suite, *ACM Trans. Math. Software* **26** (4) (2000) 465-519.
- [30] N. Bellomo, E. De Angelis, L. Graziano, and A. Romano, Solution of Non-linear Problems in Applied Sciences by Generalized Collocation Methods and Mathematica, *Comput. Math. Appl.*, **41** (2001) 1343-1363.
- [31] R. Revelli and L. Ridolfi, Sinc Collocation-Interpolation Method for the Simulation of Nonlinear Waves. *Comput. Math. Appl.* **46** (2003) 1443-1453.

-
- [32] F. Stenger, *Numerical Methods Based on Sinc and Analytic Functions*, Springer-Verlag, New York, 1993.
- [33] R. D. Skeel, and M. Berzins, A Method for the Spatial Discretization of Parabolic Equations in One Space Variable, *SIAM Journal on Scientific and Statistical Computing* **11** (1990) 1–32.
- [34] G. D. Smith, *Numerical Solution of Partial Differential Equations: Finite Difference Methods*, 3rd ed., Clarendon Press, Oxford, 1985.
- [35] E. Momoniat, R. Ravindran and S. Roy, The influence of slot injection/suction on the spreading of a thin film under gravity and surface tension, Preprint submitted to Elsevier Science 12 November 2007.